Influence of the synthesis conditions of γ-alumina on its hydrocarbons and water adsorption properties

Solange Rafaela de Jesus Borrego

Thesis to obtain the Master of Science Degree in

Chemical Engineering

Supervisors

Dr. Karin Barthelet (IFPEN)
Dr. Elsa Jolimaître (IFPEN)
Matthieu Lagauche (IFPEN)
Prof. Eduardo Jorge Morilla Filipe (IST)

Examination Committee

President: Prof. Benilde de Jesus Vieira Saramago (IST)
Supervisor: Prof. Eduardo Jorge Morilla Filipe (IST)
Members of the Committee: Prof. Moisés Luzia Gonçalves Pinto (IST)

October 2015

This page is intentionally left blank.

“The great thing about science is that you can get it wrong over and over again, because what you’re after — call it truth or understanding — waits patiently for you. Ultimately, you’ll find the answer, because it doesn’t change.”

Dudley Herschbach (Winner of the 1986 Nobel Prize in Chemistry)

Acknowledgments

Throughout this internship, I was able to learn more than I could have ever imagined, and that would have not been possible without the support of everyone. Thank you to Professor Filipa Ribeiro, who helped me throughout the application process and applying in the first place to IFPEN. I would also like to thank Joana Fernandes and Vitor Costa for all the support during the internship.

To my supervisors at IFPEN, Karin Barthelet and Elsa Jolimaître, who throughout six months were very supportive and patient, I want to show appreciation for the invaluable opportunity I was given. It was a very enjoyable experience, because I was surrounded by such kind, capable people.

My internship was integrated in Matthieu Lagauche's thesis, and to him I owe my most heartfelt gratitude: the way he so quickly integrated me in the project, his unquestionable availability, patience, and kindness were professionally and personally an absolute joy to work with; the success of this internship is in large part due to him.

To Céline Chizallet and Kim Larmier, who so caringly gave us much information about DFT, thank you very much for your help.

I want to thank also Professor Eduardo Filipe, for the support given during this internship all the way from Lisbon.

It is also important to thank everyone at the R061 department, who from the very beginning were extremely nice to me, and very patient with my French.

To the other Portuguese interns (Joana, Ana, Casinhas, Loios, Catarina, David, Diogo), you guys were a family to me throughout this time. Thank you so much for the great moments we were able to have together; I will cherish them greatly.

To the other former/current workers/interns/thésards at IFPEN (Mafalda, Pedro, Larissa, Alexis, Raido, Ana Rita, Max, Sónia, Leonor, Rúben, Leonel, Marisa, Fabien, Dina, and many others) who were so great to me all this time, thank you for your support as well.

To my friends back in Portugal who were so excited about me going abroad (Débora, Marta, Luísa, Raisa, Teresa, Nádia), thank you always for your unconditional love all these years.

And last, but definitely not least, to my parents and close family, who through a message or a phone call always kept my spirits up while I was in Lyon; to my mother, who is the greatest woman in this world; to my brother, who is the greatest man in this world; and to my nephew, who is the greatest little boy in this world.

Abstract

The surface properties of γ-alumina, the most used support in heterogeneous catalysis, can be changed by its synthesis and/or pretreatment conditions. Since water adsorbs dissociatively on the surface of γ-alumina, its surface state will depend also on the water partial pressure of the atmosphere. However, those surface properties have never been clearly correlated to the adsorption properties of γ-alumina. Since adsorption is the first step of every catalytic reaction, this could be interesting information to get, being the objective of this study.

To reach this objective, different γ-alumina samples were synthesized: two from a boehmite named Pural SB3 changing the nature of the synthesis gas, and another one from a boehmite named Disperal 40 to study the influence of the boehmite morphology. They were characterized in terms of water adsorption and, for one of them, of hydrocarbons adsorption by thermogravimetry.

Extensive study on the first sample (Pural SB3 decomposed under air) showed that adsorption isotherms can only be obtained through adsorption measurements, which were simulated by a model based on DFT, and by a normal-like distribution model, with good fittings. The equilibrium cannot be reached by desorption, because the desorption activation energy of the last hydroxyls is too high. Changing the synthesis gas from air to nitrogen resulted in an unstable sample, but starting from a boehmite with bigger particles with proportionally fewer edges lead to a sample with less adsorption capacities, which suggests that edges are important adsorption sites for water. Finally, a preliminary hydrocarbons adsorption study was conducted on the first sample, showing that ethylene adsorbs more than ethane, and that its adsorption capacity increases with the decrease of hydroxyls content. In particular, desorbing the last hydroxyl seems to free a specific site that has now to be identified.

This study gives encouraging results that have now to be completed.

Keywords: γ-alumina; water adsorption; hydrocarbons adsorption; synthesis conditions

Resumo

As propriedades de superfície da γ-alumina, o suporte mais utilizado em catálise heterogénea, podem ser modificadas pelas suas condições de síntese e/ou pré-tratamento. Uma vez que a água se adsorve de maneira dissociativa na superfície da γ-alumina, o estado da sua superfície vai ainda depender da pressão parcial da água na atmosfera. No entanto, essas propriedades de superfície nunca foram claramente relacionadas com as propriedades de adsorção da γ-alumina. Como a adsorção é o primeiro passo de qualquer reacção catalítica, esta informação é interessante, sendo o objectivo deste estudo.

Para alcançar este objectivo, sintetizaram-se várias amostras diferentes de γ-alumina: duas a partir da boemite Pural SB3, mudando a natureza do gás de síntese; e outra a partir da boemite Disperal 40, de forma a estudar a influência da morfologia da boemite. Estas amostras foram caracterizadas em termos de adsorção de água e, para uma delas, de adsorção de hidrocarbonetos por termogravimetria.

Um estudo extenso na primeira amostra (Pural SB3 calcinada sob ar) mostrou que as isotérmicas de adsorção de água só podem ser obtidas através de medidas de adsorção, que foram modeladas usando DFT e ainda recorrendo a um modelo de distribuição normal, com bons ajustes. Não é possível atingir o equilíbrio por dessorção, uma vez que a energia de activação da dessorção dos últimos hidroxilos é muito alta. Mudar o gás de síntese de ar para azoto resultou numa amostra instável, mas começar de uma boemite com um menor número de cantos resultou numa amostra com menor capacidade de adsorção, sugerindo que os cantos são sítios de adsorção importantes para a água. Finalmente, foi feito um estudo preliminar da adsorção de hidrocarbonetos na primeira amostra, mostrando que o etileno adsorve menos do que o etano, e que a sua capacidade de adsorção aumenta com a diminuição de hidroxilos à superfície. Em particular, dessorver o último hidroxilo parece libertar um sítio específico que tem agora de ser identificado.

Este estudo tem resultados encorajadores que devem agora ser completados.

Palavras-chave: γ-alumina; adsorção de água; adsorção de hidrocarbonetos; condições de síntese

Table of contents

List of figures

List of tables

1. Introduction/Objectives

Transition aluminas are metastable crystalline phases usually obtained through the thermal decomposition of boehmite. They have a very important role in the chemical and refining industry, being used in processes as diverse as ammonia production, hydrocracking, and catalytic reforming as heterogeneous catalysts and supports.

γ-alumina is a low-temperature transition phase, and the aluminum oxide used the most as a support in the chemical industry due to its attractive qualities: very high porosity, surface area, acid/base characteristics, and relative inexpensiveness.

Many studies put in evidence that the synthesis conditions of γ-alumina have an important effect on its surface structure and, by extension, on its textural and chemical properties. The number and type of hydroxyls present at the surface of γ-alumina are closely related to these properties, with a variety of models having been proposed since the 1960s that describe the surface of γ-alumina by interpreting the corresponding IR and NMR spectra. However, it still does not exist a well-established correlation between these properties and the activity of catalysts made from these supports.

Since adsorption is the first chemical step of the catalytic process, and potentially a limiting one with heavy influence on catalytic activity, it is an interesting problem to try to find a correlation between the surface of γ-alumina and its adsorption capacity of hydrocarbons.

The objective of this work consisted in preparing aluminas with different surfaces by varying their synthesis conditions (structure of the initial boehmite, type of gas, and water content in the gas), in order to study the corresponding water adsorption properties to be able to modulate the nature of the surface. Finally, the study of hydrocarbons adsorption was planned, but due to lack of time, just a few experiments have been made.

2. State of the art

2.1. General considerations

The role of chemical processes is to transform feedstock into useful products by means of a reactor, that is, the equipment where chemical reactions take place. The efficiency of this equipment conditions the entire process, which is why it is of utmost importance this parameter is optimized to the best of our knowledge.

If a chemical process is meant to be implemented on an industrial scale, the chemical reactions involved have to be fast; on the other hand, the process has to be selective in order to obtain the desired product if there are other products that can be formed. Using catalysts allows us not only to raise the rate of the chemical transformations concerned, but also to focus the process to the formation of the wanted product. Therefore, catalytic processes are more efficient not only in terms of costs, since there is less consumption of energy and feedstock, but also in environmental terms, due to less production of undesirable byproducts. In fact, catalysts are used in more than 80% of all chemical industry processes, being fundamental to the sustainable development of the economy and quality of life.

Considering a hypothetical exothermic reaction where the reagents X and Y give the product Z and analyzing the corresponding potential energy diagram (Figure 2.1), it is apparent that introducing a catalyst in the system gives way to a new reaction pathway that requires a lower activation energy (E_a) than the non-catalyzed reaction; thus, there is an increase of the reaction rate, and the catalyzed reaction is more energetically favorable. Since the initial and final states remain unchanged, the variation of free energy (ΔG) is the same, and the chemical equilibrium is not altered because of the catalyst.

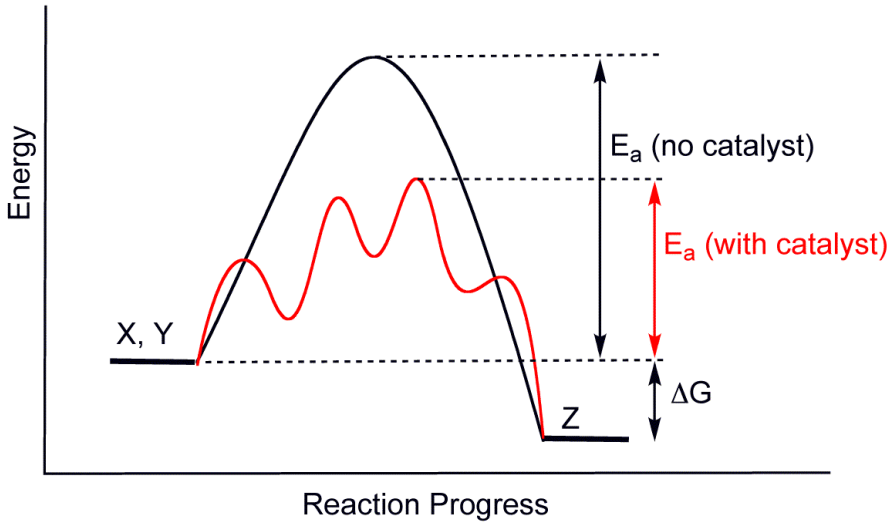

Figure 2.1 – Potential energy diagram for the exothermic reaction X + Y → Z [1].

Heterogeneous catalysis occurs when the catalyst, reagents, and products are in different phases; usually, the former is on the solid state, while the latter are on the gaseous or liquid states. This type of catalysis has the key advantage of it being relatively simple to separate the catalyst from the product stream, which is very important for continuous chemical processes.

2.2. γ-alumina

2.2.1. Transition aluminas

Transition aluminas (Al_2O_3) are very important heterogeneous catalysts and supports, being used in processes as diverse as ammonia production, hydrocracking, catalytic reforming, isomerization, and the Claus process. They are obtained by the calcination of aluminum hydroxides. Starting from different hydroxides leads successively to several forms with different thermal stability, surface acidity, and textural properties (Figure 2.2).

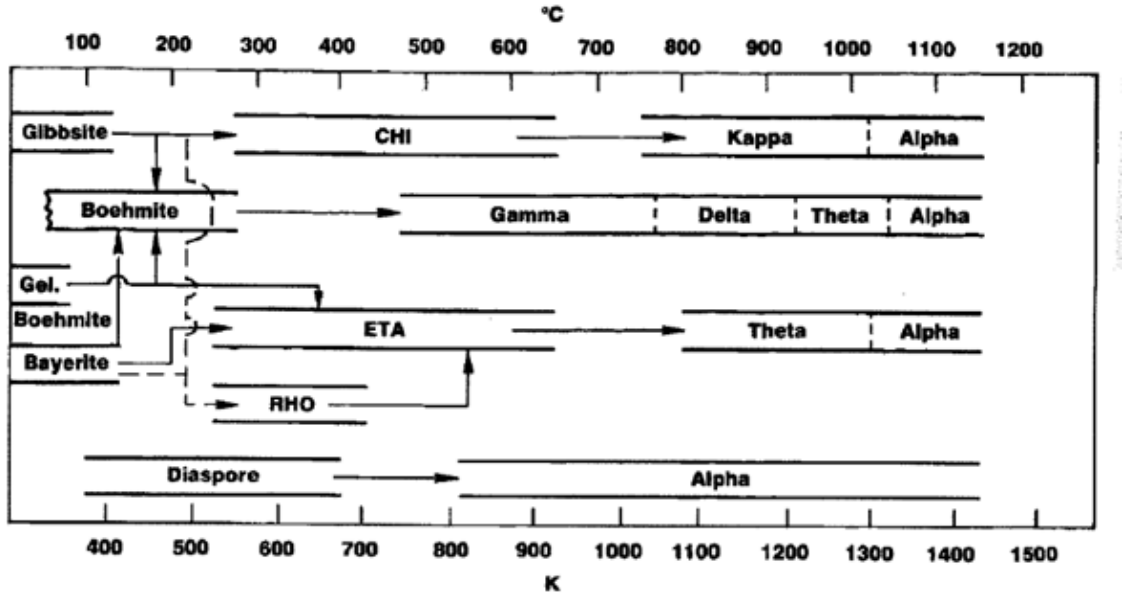

Figure 2.2 – Transformation of aluminum hydroxydes in different aluminas [2].

Low-temperature transition aluminas (synthesized below 750°C) are more active than high-temperature ones, which is explained by their higher surface area, and number of surface active sites.

Among aluminum hydroxides, boehmite (aluminum oxyhydroxide, AlOOH), is an important precursor because it leads to γ-alumina, the aluminum oxide used the most as a support. In fact, 90% of the supports used in heterogeneous catalysis are made of γ-alumina [3], due to its very high porosity, surface area, and acid/base characteristics.

2.2.2. Synthesis of γ-alumina

The boehmite calcination to form transition aluminas involves short-range rearrangements of atoms in the crystal structure (topotactic transformation); thus the cubic packing of oxygen sub lattice of boehmite is maintained in the γ-alumina (Figure 2.3). The temperatures at which γ-alumina is formed are variable, depending on the crystallinity of the boehmite precursor and the thermal treatment conditions. As such, the microscopic morphology of the boehmite precursor has a major influence on the characteristics of the transition aluminas, such as the specific area, porosity, pore-size distribution, and acidity [4].

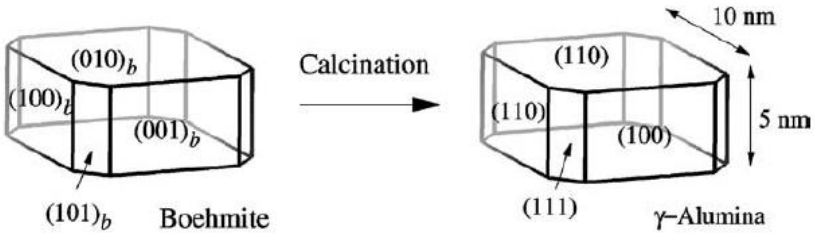

Figure 2.3 – Topotactic transformation of boehmite into γ-alumina [5].

2.2.3. Surface and structure of γ-alumina

The surface properties of γ-alumina are related to local microstructure and surface chemical composition, and can be manipulated in order to govern the acid-basic reactions and the dispersion of active phases on the support. There is wide experimental evidence that all of these properties are dependent on the preparation step [6].

The surface and structure of γ-aluminas have been a subject of study since the 1960s, aided by technologies such as infrared spectroscopy [7–10], nuclear magnetic resonance spectroscopy [8,9,11], and x-ray diffraction [9,11,12].

Lippens *et al.* [13] studied the structure of γ-alumina using crystallography, and concluded that it has three types of crystallographic faces in the directions (100), (110), and (111) of the cubic spinel structure (Figure 2.4), which is the usual structure that is associated with γ-alumina. This structure contains eight patterns AB_2O_4, where the A atoms are in tetrahedral sites, while the B atoms are in octahedral sites.

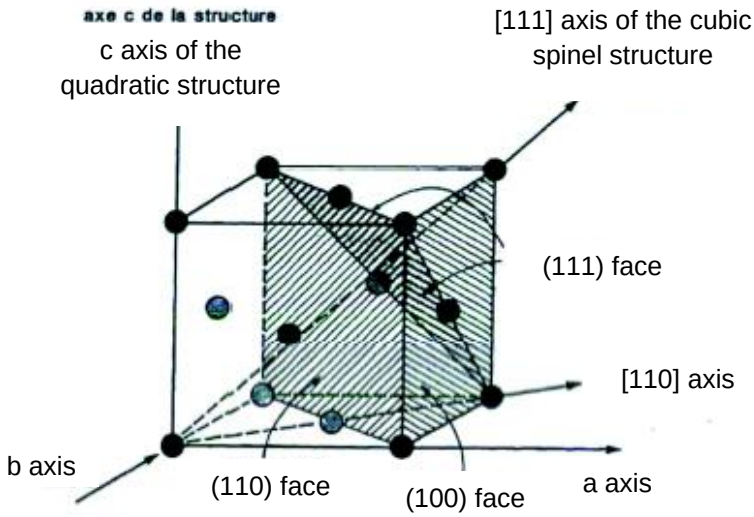

Figure 2.4 – Crystallographic faces of γ-alumina [14].

The experimental unit cell for the structure of γ-alumina is represented on Figure 2.5. γ-aluminas have a defective nature due to the presence of only trivalent Al cations in the spinel-like structure. The Al atoms occupy the octahedral and tetrahedral sites, while there is a cubic close-packed stacking of oxygen layers next. To ensure electrical neutrality, there are vacancies in some lattice positions. Their

exact location is still a matter of debate: some authors have studied γ-aluminas using x-ray diffraction, nuclear magnetic resonance spectroscopy, and transmission electron microscopy, concluding that these vacancies occur mostly in octahedral sites with the Al cation in tetrahedral sites [15,16], while others have concluded they occur mostly in tetrahedral sites [8,17]. It has also been suggested that these vacancies should be thought of as randomly distributed between tetrahedral and octahedral positions [18].

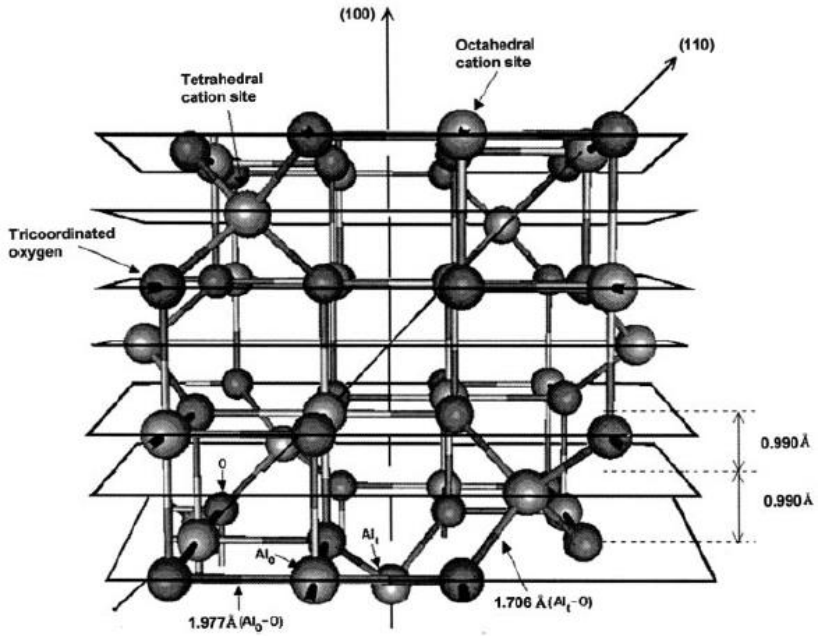

Figure 2.5 – Experimental cubic γ-alumina spinel-type unit cell [19].

Though their exact distribution is still not completely clear, it is expected that these vacancies occur also at the surface of γ-aluminas. In addition, there are at the surface coordinatively unsaturated (*cus*) cations, with the coordination number of aluminum being tetrahedral (Al^{IV}) or octahedral (Al^{VI}) [9,10,20], with variable amounts of pentahedrally coordinated aluminum (Al^{V}) also being reported [7,8,21,22]. These facts are responsible for the elaborate and heterogeneous surface typical of γ-alumina.

The most abundant component at the surface of γ-alumina is made up of water, that can adsorb by two means: undissociated (H_2O), or dissociated in the form of hydroxyls (OH^-); this adsorption occurs to compensate the surface unsaturation present at the uppermost layer due to the presence of coordinatively unsaturated cations and anions [23]. The hydroxyls at the surface of γ-alumina have a major influence on its chemical and electrochemical properties, and as such any process that modifies the hydroxyls coverage on γ-alumina, such as the temperature of calcination, can have an effect on the surface state [6].

2.2.3.1. Surface hydroxyls

Infrared spectroscopy is a way to study the structure of the surface of γ-alumina thanks to the characterization of the hydroxyls present on it (example in Figure 2.6). Indeed, in function of the

coordination number of aluminum, and the number of aluminums the hydroxyl is bonded to (hydroxyls can be terminal, bridged or tribridged), the hydroxyl will have a distinct frequency.

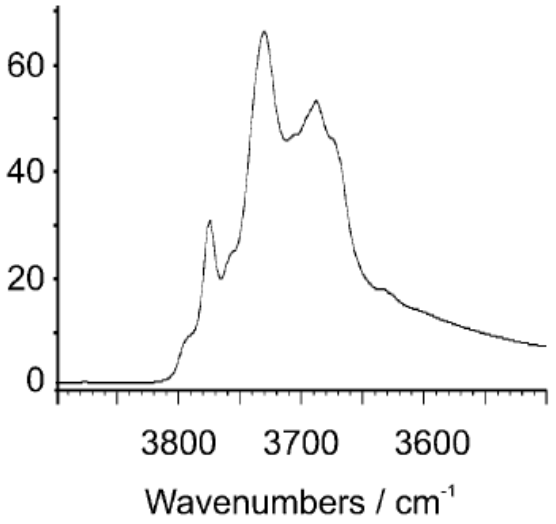

Figure 2.6 – Infrared spectrum of γ-alumina dehydroxylated at 500ºC [23].

To try to attribute each band on the infrared spectra, several surface models have been successively developed since 1965. Among the first ones was one developed by Peri [24]. It was followed by another one developed by Tsyganenko [25], who proposed for the first time a double coordination of Al ions in γ-alumina. This was considered partly responsible for the multiplicity of OH bands observed in the corresponding spectra. As such, there are three types of hydroxyl groups, represented on Figure 2.7, called type I (terminal), type II (bridged), and type III (tribridged).

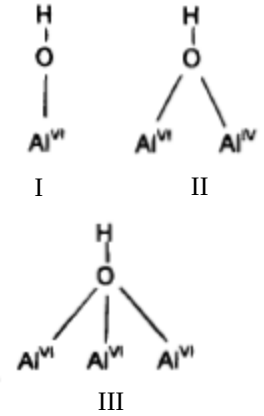

Figure 2.7 – Three types of hydroxyls that occur at the surface of γ-aluminas, according to Tsyganenko's model [23].

In 1978, Knözinger and Ratnasamy [24] proposed a model that relates the previous ones to describe five types of hydroxyls present on the surface of γ-alumina: depending on the Al coordination and the number of Al neighbors, these groups present a distinct net electric charge (Figure 2.8), that characterizes the strength and acid/basic characteristics of the OH bond, with acidity increasing with the net charge of the molecule. The number of different configurations described in this model corresponds to the number of OH components observed in the spectrum of γ-alumina.

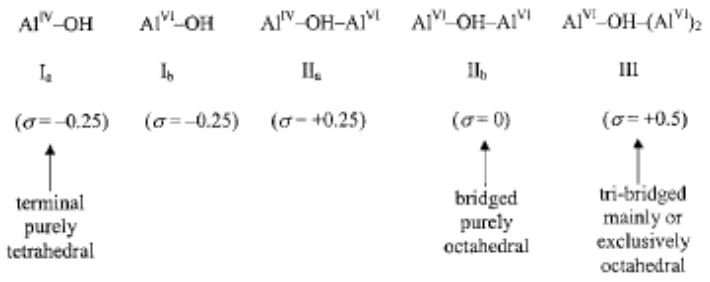

Figure 2.8 – Five different types of OH configurations at the surface of γ-alumina according to Knözinger's model [6].

Although this is currently the most frequently used empirical model for describing the surface of γ-alumina, it is, in fact, an elementary model, since it does not take into account the crystallographic type of the surface, its state (hydroxylated or dehydrated) that is temperature-dependent, neither the possible influence, at the surface, of some of the cation vacancies imposed to the spinel structure due to stoichiometry. To compensate these lacks, Digne *et al.* [25] developed a realistic surface model based on the Density Functional Theory (DFT) for the dehydrated surface of γ-alumina considering the crystallographic plan, and the temperature effects on the hydroxyl surface coverage (Figure 2.9 and Figure 2.10). It was determined that the behavior of various types of surface hydroxyl groups depends strongly on the local chemical environment, morphology (exposed surfaces), and composition of the oxide.

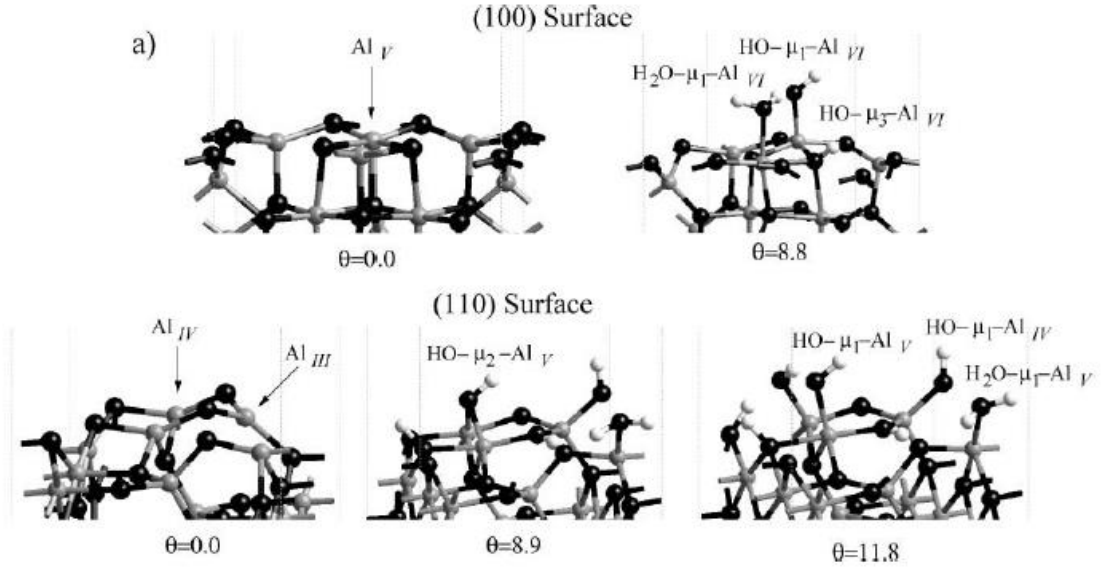

Figure 2.9 – Relaxed configurations of a) γ-alumina (100) and b) γ-alumina (110) surfaces for different hydroxyl coverage (θ in OH/nm^2) [25].

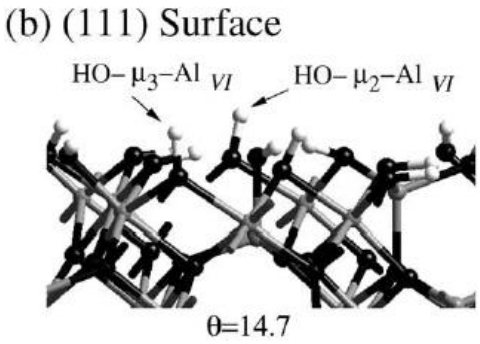

Figure 2.10 – Totally hydrated surface of γ-alumina (111) [26].

When the nature of the hydroxyls present at the surface is determined, it is possible to calculate their vibration energies, where each site has its own frequency [25]. The infrared frequencies and corresponding sites according to this and the other models can be found on Table 2.1.

Table 2.1 – Average IR frequency and sites according to Peri, Tsyganenko, and Knözinger for a γ-alumina obtained at 500°C [23,25].

OH band	Average frequency (cm^{-1})	Peri's assignment	Tsyganenko's assignment	Knözinger's assignment	DFT assignment
1	3800	A	I	Ib (oct.)	HO-μ_1-Al^{IV} (110)
2	3775	D	I	Ia (tetra.)	HO-μ_1-Al^{VI} (100)
3	3745	B	II	IIb (oct.-oct.)	HO-μ_3-Al^{VI} (111)
4	3730	E	II	IIa (oct.-tetra.)	HO-μ_1-Al^{IV} (100)
5	3710	C	III	III	HO-μ_2-Al^{VI} (110)
6	3690	C	III	III	HO-μ_2-Al^{VI} (111)
7	3590	H-bonded	--	H-bonded	HO-μ_3-Al^{VI} (100)

2.2.4. Sum-up

Thanks to a variety of appealing qualities, γ-alumina is the most used support in heterogeneous catalysis. Its surface properties are correlated to the surface state, which heavily depends on the synthesis conditions applied, that change its hydration state. The surface hydroxyls have been studied by several techniques, such as IR spectroscopy, and modeled based on DFT. Many authors agree to distinguish hydroxyls in function of the coordination number of the aluminum they are bonded to, and the number of aluminum neighbors.

2.3. Adsorption

The heterogeneous chemical reaction takes place on the interface solid-fluid, and the chemical catalytic cycle steps (Figure 2.11) are, in broad outline, as follows:

1. Adsorption of the reagents on available active sites;
2. Surface reactions involving formation or conversion of various adsorbed intermediates;
3. Desorption of the products.

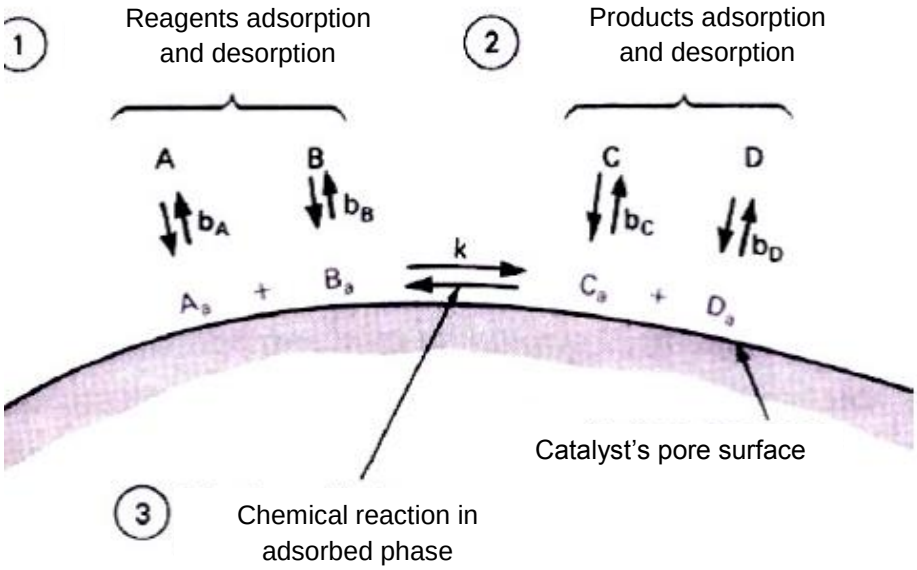

Figure 2.11 – Solid-fluid interface of a heterogeneous catalytic reaction [27].

The adsorption of the reagents on active sites is the first chemical step of any catalytic cycle, promoting the weakening of the bonds of the molecules of reagents, making their conversion in products smoother. It is defined by IUPAC [28] as "an increase in the concentration of a dissolved substance at the interface of a condensed and a liquid phase due to the operation of surface forces." It is a surface phenomenon by which the atoms or molecules of gases or liquids, called adsorbates, fix themselves on a solid surface, the adsorbent, through more or less intensive processes. It is possible to distinguish between two different types of adsorption depending on the nature of the forces involved:

1. Chemisorption – covalent forces: there is the formation of chemical bonds, which in turn means that the heat of adsorption is high, in the same order of magnitude as the heat of reactions (40-400 kJ/mol) [29]. The molecules form no more than a monolayer (Figure 2.12, to the left), and the strength of the bonds decreases as the surface starts to get full. This kind of adsorption can be dissociative, when the adsorbed molecule dissociates in two or more fragments that bond to the surface, or non-dissociative, when the molecule is adsorbed as it is;
2. Physisorption – van der Waals forces: there is no chemical modification of the adsorbed molecules, and the heat of adsorption is low, in the same order of magnitude as the heat of

condensation (20-40 kJ/mol) [29]. The molecules arrange themselves in multilayers (Figure 2.12, to the right), and the strength of adsorption gets weaker as the number of layers increases.

Table 2.2 gives compiled information about the differences between chemisorption and physisorption.

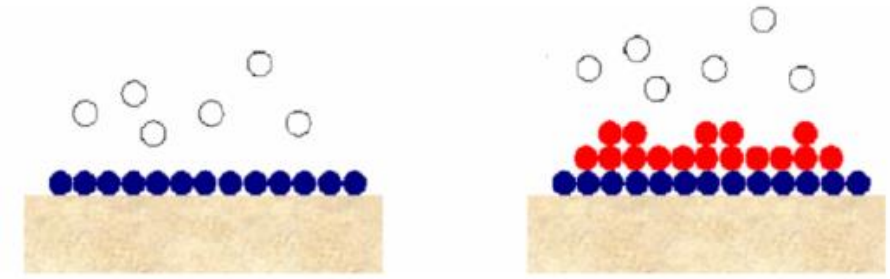

Figure 2.12 – Monolayer and multilayer adsorption [29].

Table 2.2 – Differences between physisorption and chemisorption [29].

	Physical adsorption	Chemisorption
Specificity	unspecific	specific
Number of adsorbed layers	> 1	Max 1
Adsorption heat, ΔH_{ads} (kJ/mol)	20-40	40-400
Rate of adsorption	high	relatively low
Desorption	by decreasing pressure	by increasing temperature

The potential energy of physisorption and chemisorption can be represented using the Lennard-Jones diagram, exemplified in Figure 2.13 for the adsorption of a diatomic gas X_2 over a metal M, where the curve P shows the interaction between M and X_2, and the curve C shows the behavior of chemisorption when the molecule suffers a dissociation to 2X.

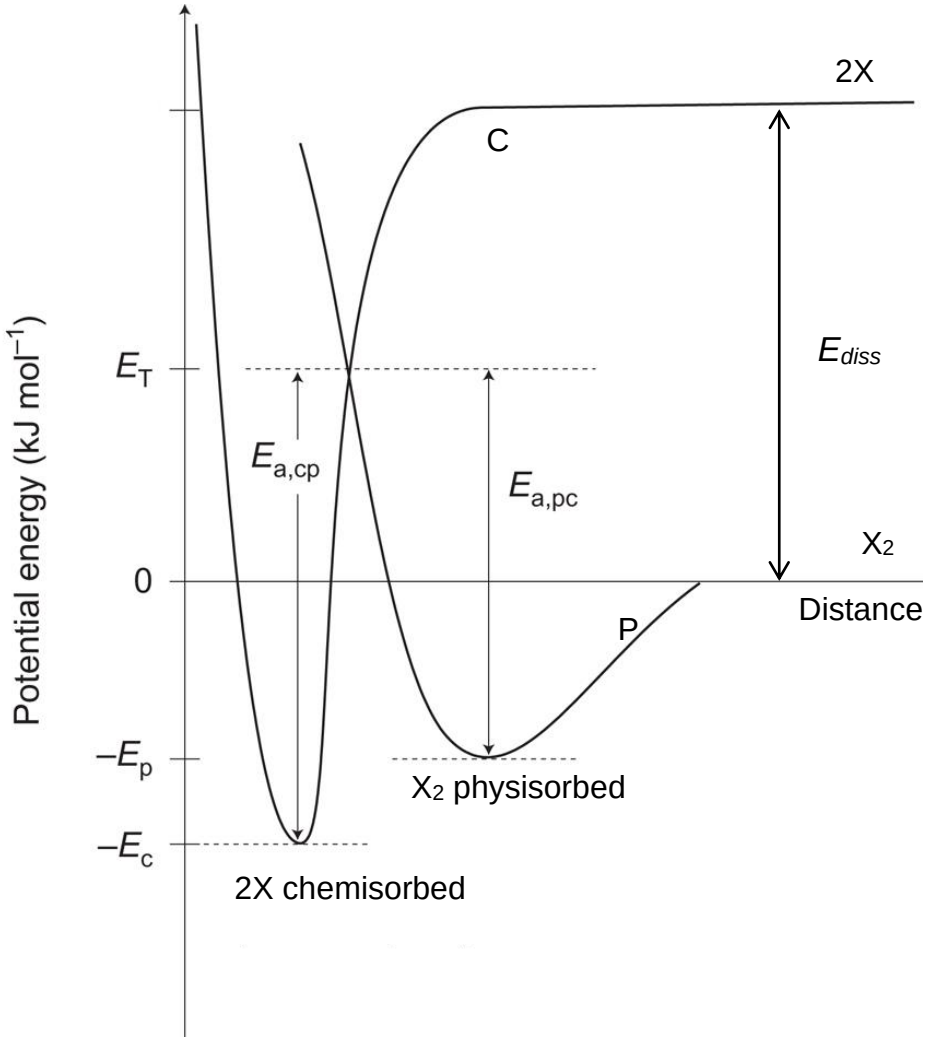

Figure 2.13 – Lennard-Jones potential energy diagram for the adsorption of a diatomic gas over a metal [30].

In the absence of physisorption, it would be necessary to activate the gas molecules by providing them with an amount of energy equal to the dissociation energy, which is very high. Hence, the molecules get physisorbed at first, which means that they approach the surface of the metal following a low energy path. On the intersection between the two curves (C and P) occurs the transition to chemisorption. In this example, this transition point occurs above the x axis, which indicates chemisorption is activated. Nonetheless, that activation energy is still much lower than the dissociation energy of the molecule.

Due to the activation energy, chemisorption is usually very slow at low temperatures. On the other hand, the rate of physisorption decreases fast when the temperature increases, and it is usually very small for temperatures above the critical temperature.

2.3.1. Adsorption thermodynamics

Adsorption is a spontaneous process ($\Delta G_{ads} < 0$), and since when the molecules of the adsorbate go from the free gas to the adsorbed film they lose one degree of translational freedom, the variation of entropy is negative ($\Delta S_{ads} < 0$). According to (2.1), the variation of enthalpy has, then, to be negative

($\Delta H_{ads} < 0$), which is to say that adsorption is an exothermic process: when the temperature decreases, the quantity of adsorbed molecules in the equilibrium increases.

$$\Delta G_{ads} = \Delta H_{ads} - T\Delta S_{ads} \tag{2.1}$$

Where:

ΔG_{ads} – Variation of Gibbs free energy of adsorption (kJ/mol);

ΔH_{ads} – Variation of adsorption enthalpy (kJ/mol);

T – Temperature (K);

ΔS_{ads} – Variation of adsorption entropy (kJ/(mol.K)).

In the cases of reactive systems with variation of quantity of reagents and products in the system, the chemical potential in each phase is often used. It is defined by (2.2) and (2.3), considering that there are no changes to the thermodynamic properties of the solid surface upon adsorption.

$$\mu_a = \left(\frac{\partial G_a}{\partial n_a}\right)_{T,P} \tag{2.2}$$

$$\mu_g = \left(\frac{\partial G_g}{\partial n_g}\right)_{T,P} \tag{2.3}$$

Where:

$\mu_{a,g}$ – Chemical potential in adsorption and desorption, respectively (kJ/mol);

$n_{a,g}$ – Number of moles of gas in adsorption and desorption, respectively (mol).

Keeping the temperature constant and adjusting the pressure of the system by adding dn_g molecules of gas, the two phases are not in equilibrium, and matter will be transferred in the direction of lower free energy, which leads to adsorption. An equilibrium is reached eventually, and the chemical potential of the two phases are equal (2.4).

$$dG = (\mu_a - \mu_g)dn_a = 0$$
$$\mu_a = \mu_g \tag{2.4}$$

The chemical potential can also be expressed in terms of concentration (2.5), and it follows that the equilibrium constant is given by (2.6).

$$\mu_g = \mu_g^0 + RTln\left(\frac{P_A}{P_0}\right) \tag{2.5}$$

$$K_A = \frac{P_0}{P_A} \times \frac{a_{s,A}}{a^0} \tag{2.6}$$

Where:

μ_g^0 – Standard chemical potential of the gas at the reference pressure P_0, for a given temperature (kJ/mol);

R – Ideal gas constant (8,32 J/(mol.K));

P_A – Partial pressure of the gas A (Pa);

K_A – Equilibrium constant for adsorption of the gas A;

$a_{s,A}$ – Activity of gas A in the adsorbed phase.

2.3.2. Adsorption isotherms

The adsorption equilibrium can be expressed by an adsorption isotherm, which represents the amount of adsorbed adsorbate on the solid in the equilibrium as a function of the equilibrium relative pressure, p/p°, where p^0 is the saturation pressure of the pure adsorbate at the temperature of measurement, at a fixed temperature. The adsorption isotherm is one of the most important criteria for an adsorption process, since the adsorption capacity, or uptake, of a given catalyst should favor its efficiency.

The form of the adsorption isotherm offers information about the properties of the catalyst material and about the way the adsorption process is led over a certain surface. It is possible to divide the adsorption isotherms into six types (Figure 2.14). All of them, at sufficiently low surface coverage, take a linear form: this is called the Henry's Law region.

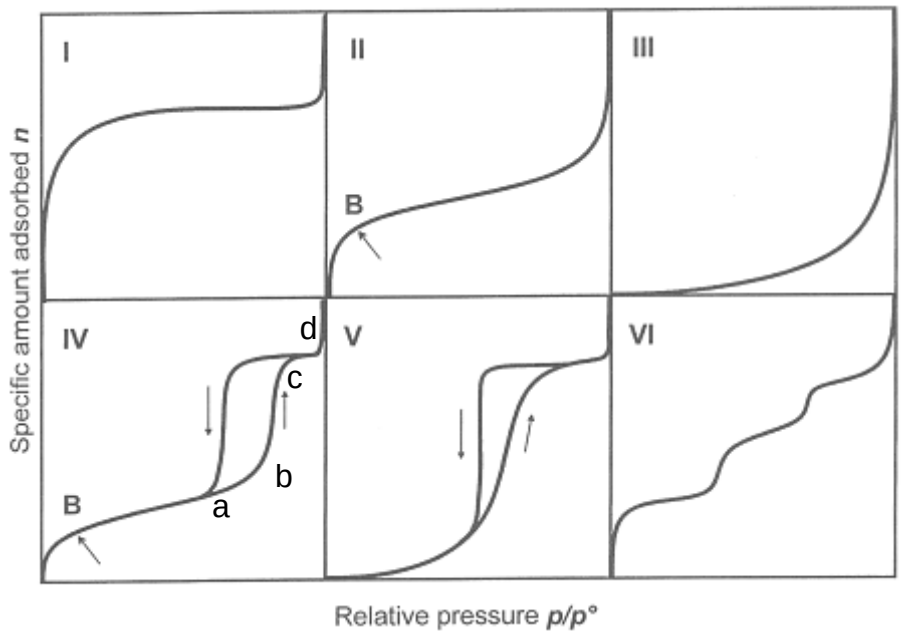

Figure 2.14 – Types of adsorption isotherms according to IUPAC [28].

1. Type I isotherms are reversible and depict monolayer adsorption. They are typical of microporous solids which possess small external surfaces, as is the case for molecular sieve zeolites, and the accessible micropore volume is what limits the maximum amount that can be adsorbed;
2. Type II isotherms are reversible and typical of non-porous or macroporous adsorbents, and represent unrestricted monolayer-multilayer adsorption. The signaled point (B), that marks the beginning of the almost linear middle section of the isotherm, is where the monolayer is complete, and multilayer adsorption begins;

3. Type III isotherms are reversible and contain only the multilayer, typical of weak adsorbent-adsorbate interactions when compared to adsorbate-adsorbate interactions. They are not very frequent;
4. Type IV isotherms are typical of many mesoporous industrial adsorbents, with capillary condensation occurring in the mesopores. The first part of this isotherm is assigned to monolayer-multilayer adsorption, since it follows the same path as the corresponding part of a Type II isotherm;
5. Type V isotherms are not common, and are associated with Type III isotherms, since the adsorbent-adsorbate interactions are also weak, but they are obtained with certain porous adsorbents;
6. Type VI isotherms are typical of multilayer adsorption on a uniform non-porous surface, where each step denotes the monolayer capacity for each adsorbed layer.

The capillary condensation that can be observed in all types of isotherms except Type I is the phenomenon of condensation of the vapor below the saturation vapor pressure of the pure liquid. It occurs in small pores, that is to say, in a confined space. The critical pore size under which the capillary condensation occurs depends on the wetting of the adsorbate. These two parameters are linked thanks to the Kelvin Law (2.7).

$$ln\frac{p}{p^0} = \frac{2\gamma V_m}{rRT} \quad (2.7)$$

Where:
p – Vapor pressure (Pa);
p_0 – Saturation vapor pressure (Pa);
γ – Surface tension (J/m^2);
V_m – Molar volume of the liquid (m^3/mol);
r – Radius of the droplet (m).

Capillary condensation is a reversible phenomenon, but desorption of the condensate adsorbate could happen at a lower pressure than the condensation. This is called the hysteresis loop, which can be seen in the type IV isotherms. Indeed, after this condensation, there is the formation of a meniscus at the interface between the liquid and the vapor, allowing an equilibrium below the saturation vapor pressure [31], and thus the critical pore size becomes two times lower than the one during adsorption.

The adsorption isotherms can be obtained by experimental data, and various models can be used to fit that data accordingly.

- *Langmuir model*

The quantitative treatment of the adsorption/desorption equilibrium was first done by Langmuir [32] in 1916, who devised a very simple model based on these assumptions:

- The surface of the adsorbent is uniform, which means that all the active sites are equivalent;
- Adsorbed molecules do not interact between them;
- All adsorption occurs through the same mechanism;
- At maximum adsorption, only a monolayer is formed.

Representing the active sites by *, and considering that each molecule A occupies only one active site, the adsorption/desorption equilibrium can be given by (2.8).

$$A + * \Leftrightarrow A* \tag{2.8}$$

When there is a dynamic equilibrium between the molecules in the fluid phase and the adsorbed adsorbate on the active centers at the surface, the rate of adsorption and desorption are equal and (2.9) is true, where the rate constants related to adsorption and desorption are given by (2.10) and (2.10).

$$k_a P_A (1 - \theta_A) = k_d \theta_A \tag{2.9}$$

$$k_a = A_a exp\left(-\frac{E_a}{RT}\right) \tag{2.10}$$

$$k_d = A_d exp\left(-\frac{E_d}{RT}\right) \tag{2.11}$$

Where:

$k_{a,d}$ – Reaction rate constant of adsorption and desorption, respectively (s^{-1});

Θ_A – Surface coverage (g/g);

$A_{a,d}$ – Pre-exponential factor for adsorption and desorption, respectively (s^{-1});

$E_{a,d}$ – Activation energy for adsorption and desorption, respectively (kJ/mol).

The adsorption equilibrium constant is given by (2.12).

$$K_A = \frac{k_a}{k_d} = \frac{A_a}{A_d} exp\left(-\frac{E_a - E_d}{RT}\right) = B exp\left(\frac{\Delta H_{ads}^0}{RT}\right) \tag{2.12}$$

Where:

ΔH_{ads}^0 – Standard variation of adsorption enthalpy (kJ/mol).

Considering the heat of adsorption independent of the fraction of sites covered by A, it is possible to get the Langmuir isotherm (2.13).

$$\theta_A = \frac{n^a}{n_m^a} = \frac{K_A P_A}{1 + K_A P_A} \tag{2.13}$$

Where:

n^a – Adsorbed quantity (g/g);

$n^a{}_m$ – Maximum adsorbed quantity (g/g).

Figure 2.15 presents various Langmuir isotherms for different values of K_A, that grow from curve *a* to *b*, which are two limiting situations: for high temperatures, $K_AP_A << 1$ and $\theta_A \sim= K_AP_A$, which means the adsorbed quantity is directly proportional to the partial pressure, and the isotherm is close to being linear (curve *a*); for low temperatures and/or high pressures, $K_AP_A >> 1$ and $\theta_A \sim= 1$, which means the monolayer is almost saturated (curve *b*).

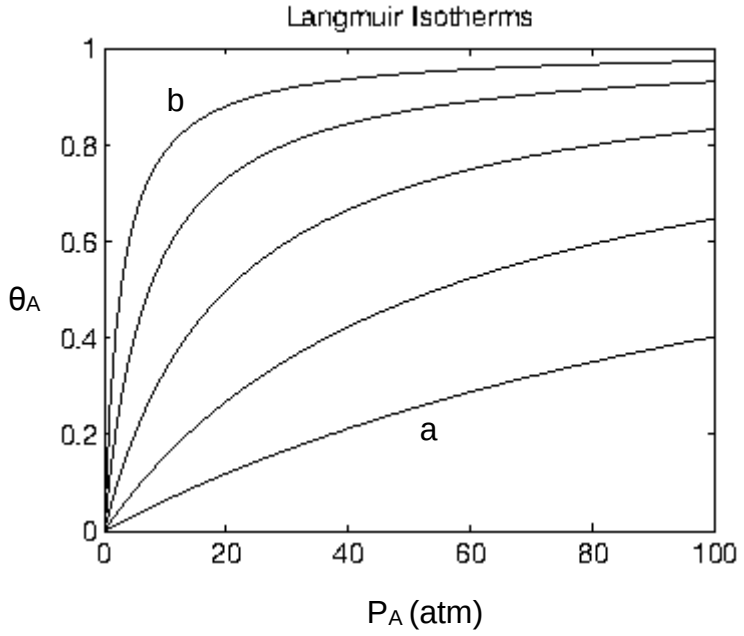

Figure 2.15 – Langmuir isotherms for different values of K_A.

The parameters associated with the model, $n_m{}^a$ and K_A, can be obtained by linear regression (2.15).

$$\frac{P_A}{n^a} = \frac{1}{n_m^a K_A} + \frac{1}{n_m^a} P_A \tag{2.15}$$

When the values of equilibrium constants at different temperatures are known, the heat of adsorption can be acquired considering the integral of the van't Hoff equation (2.16).

$$\frac{dlnK_A}{dT} = \frac{\Delta H_{ads}^0}{RT^2} \tag{2.16}$$

- *Extensions of the Langmuir model (Langmuir multisite)*

The surface of an adsorbent can be energetically heterogeneous if there are adsorption sites of different natures. This heterogeneity is often the principal cause of non-ideal behavior in adsorption systems. If independent sites z with different energies are considered, it is possible to represent adsorption by the Langmuir multisite model (2.17) [33].

$$\theta_A = \frac{K_z P_A}{1 + \sum_z K_z P_z} \tag{2.17}$$

- *BET model*

Brunauer, Emmet, and Teller (BET) developed in 1938 [34] a model whose main objective was the correct depiction of physisorption for vapors. Just like for the Langmuir model, it is assumed that there is a dynamic equilibrium between adsorption and desorption, but with the added possibility of multiple layers being adsorbed. This model makes the following assumptions:

  - On each layer, the rate of adsorption and desorption are equal;
  - The heat of adsorption is constant after the second layer and equal to the heat of condensation of the vapor;
  - When $P_A = P^0$, the vapor condenses like an ordinary liquid, and the number of adsorbed layers is infinite.

The BET isotherm is then obtained, with its linear form being represented by (2.18), where *c* is given by (2.19).

$$\frac{\frac{P_A}{P^0}}{n^a\left(1-\frac{P_A}{P^0}\right)} = \frac{1}{n_m^a c} + \frac{c-1}{n_m^a c}\frac{P_A}{P^0} \tag{2.18}$$

$$c = exp\left(\frac{E_1 - E_L}{RT}\right) \tag{2.19}$$

Where:

E_1 – Adsorption heat (kJ/mol);

E_L – Liquefaction heat (kJ/mol).

2.3.3. Water adsorption on γ-alumina

The existence of Lewis acid sites (*cus* cations) and basic sites (oxide anions) at the surface of γ-alumina allows rehydroxylation by interaction with water, with these sites being converted into surface hydroxyls. The presence of water has, then, an influence on the surface state and thus on the adsorption sites. It can also be supposed that it will compete in some cases with hydrocarbons.

All studies on rehydration of γ-alumina agree that water is initially chemisorbed and then physisorbed. Chemisorption has been evidenced in particular thanks to calorimetric measurements done by Coster *et al.* [35]: these authors consider as irreversible adsorbed quantity the one non-desorbed by a simple decrease of the pressure. They even proposed that chemisorption of water could be represented as a two-step process for γ-alumina under atmospheric conditions [35] (Figure 2.16), involving:

1. non-dissociative adsorption of water on *cus* cations, where there is a transfer of electron density to a Lewis acid site;
2. dissociative chemisorption of water and modification of surface aluminum coordination with the hydroxyl group bonded to the aluminum atom, which means that the two-coordinate oxygen atom adjacent to the aluminum site is protonated.

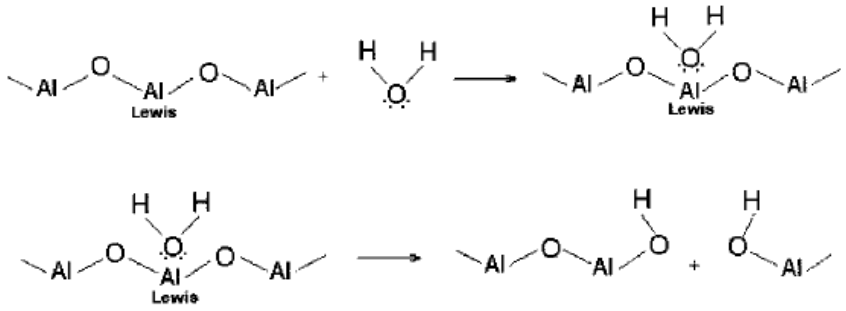

Figure 2.16 – Two-step process of the interaction between water and the surface of γ-alumina [35].

As such, chemisorbed water is not in molecular form and involves more than one type of site. On the contrary, physisorbed water involves molecular water, with hydrogen bonding to hydroxyl groups on the activated alumina surface. Depending on the pore size and relative pressure, there could also be capillary condensation within the smaller pores.

Since water is dissociatively chemisorbed, this phenomenon provokes an extensive surface reconstruction. Nuclear magnetic resonance studies done by Coster *et al.* [21] show that reconstruction by water chemisorption favors Al^{VI} at the expense of both Al^{IV} and Al^{V}, with about 60% of the surface aluminum being likely to change coordination when going through hydroxylation.

Isotherms of water adsorption on alumina are usually of type II [37], [38] (Figure 2.17).

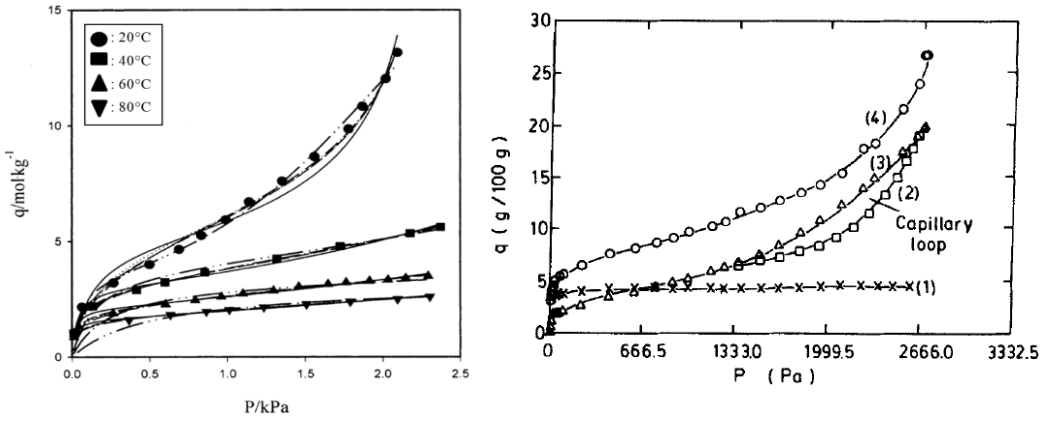

(a) Alumina activated at 320 °C during 12h [37]

(b) Isotherm at 26 °C on γ-alumina activated at 350°C under vacuum, (4) experimental and (1) to (3) simulated [38]

Figure 2.17 – Water adsorption isotherms on γ-alumina.

At low water partial pressures, the slopes of the isotherms are very high, which confirms that water adsorption is favorable in that area.

To simulate these isotherms, Ruthven *et al.* [36] divided the adsorption isotherm (4), a Type II isotherm, in many isotherms:

- Isotherm (1) corresponds to chemisorption, tending to a fixed q value of ~4 g/100 g, and is a Type I isotherm modeled by a Langmuir isotherm;
- Isotherms (2) and (3) correspond to physisorption phenomena in adsorption and desorption, with a hysteresis loop that corresponds to capillary condensation, and are modeled by a BET isotherm.

Both studies have also evaluated two models. Table 2.3 shows the values of the maximum chemisorbed value from the Langmuir model, and the maximum value of the monolayer from the BET model obtained by the models in the studies presented. Although it is difficult to comment these values because the samples used were different, the adsorption enthalpy estimated by Ruthven *et al.* is consistent with the hypothesis of chemisorption.

Table 2.3 – Results obtained by the two studies [36,37].

Study	Activation	Specific surface area, S_{BET} (m^2/g)	Maximum chemisorbed value from the Langmuir model, q_s (g/100g)	Maximum value of the monolayer from the BET model, q_m (g/100g)	Adsorption enthalpy, ΔH_{ads} (kJ/mol)
Ruthven	350°C at atm. pressure	360	3,25	3,80	- 80
Kim	320 °C in vacuum	340	5,4	7,2	_

2.3.4. Hydrocarbons adsorption on γ-alumina

Ruiz *et al.* [38] have one of the few studies available on ethane and ethylene adsorption on γ-alumina, showing a relationship between the surface coverage and the standard enthalpy, at 30°C (Figure 2.18). The adsorption enthalpy decreases with the surface coverage until reaching a value of 10 kJ/mol; this variation indicates the surface sites are not all equivalent. Ethylene presents a higher adsorption enthalpy, probably due to the interaction of the π-bond with the surface, and that difference is accentuated at low surface coverage. It seems that adsorption is more favorable for unsatured hydrocarbons, in comparison with their linear equivalents.

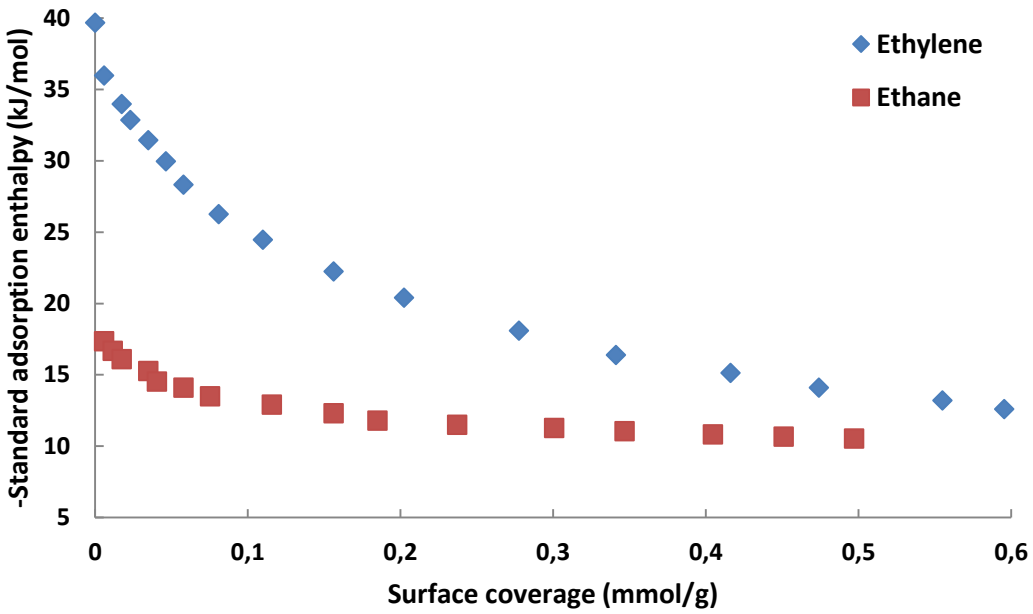

Figure 2.18 – Adsorption enthalpies for ethane and ethylene for various surface coverages at 30°C.

The adsorption enthalpies of these hydrocarbons (up to -40 kJ/mol for ethylene and -17 kJ/mol for ethane) on γ-alumina are much lower than the adsorption enthalpy of water, so it can be supposed that for ethane/ethylene, physisorption occurs. On the other hand, water would probably compete with the hydrocarbons. However, there are no studies available that validate this assumption.

2.3.2. Sum-up

Even though adsorption is the first chemical step of any catalytic cycle, and potentially a limiting one, there are not many studies available on hydrocarbons adsorption on γ-alumina. What is known is that the nature of the adsorbate, and the water content in the surrounding gas have a considerable impact on this adsorption. In particular, at low water partial pressures, water adsorption is very favorable, and there could be competition with hydrocarbons. As such, it is necessary to study water adsorption on γ-alumina in order to understand the changes in the surface state, which can have an influence on hydrocarbons adsorption.

2.4. Final conclusions and research strategy

Although γ-alumina is largely used as a catalyst support in the chemical industry, due to its textural properties, and acid/base characteristics, there is no well-established correlation between these properties and the activity of catalysts, neither between them and their adsorption capacities. To try to investigate this, different samples of γ-alumina are synthesized by varying the structure of the initial boehmite, the water partial pressure in the surrounding gas, and the type of gas. The influence of these synthesis conditions on the surface structure is studied by measuring the corresponding isotherms of water adsorption. Finally, these surface states will be correlated with their adsorption capacities of hydrocarbons.

3. Work methodology

3.1. Synthesis of γ-alumina

Various samples of γ-alumina are synthesized under different conditions, namely:

1. the type of boehmite (Pural SB3 or Disperal 40);
2. the type of gas (air or nitrogen);
3. the water content in the gas (dry or from the gas network at 230 Pa of water).

The two boehmites present different characteristics, the most important one being the ratio between the edges and plans (Figure 3.1): since the transformation of boehmite to γ-alumina is a topotactic one, that is, the crystallographic structure is maintained from reagent to product, it is interesting to compare the difference in adsorption properties and surface structure that brings about. The most important properties of the two boehmites are compared in Table 3.1.

Table 3.1 – Most important properties of boehmites Pural SB3 and Disperal 40.

Type of boehmite	Analysis	Results
Pural SB3	XRD	boehmite
	TEM	(5-40) x (3-10) x (1-3) nm
	Specific surface area, S_{BET} (m^2/g)	326
	Impurities (Cl, Na, Fe, …) (%)	< 0,01
Disperal 40	XRD	boehmite
	TEM	(10-40) x (6-30) x (2-8) nm
	Specific surface area, S_{BET} (m^2/g)	100
	Impurities (Cl, Na, Fe, …) (%)	< 0,01

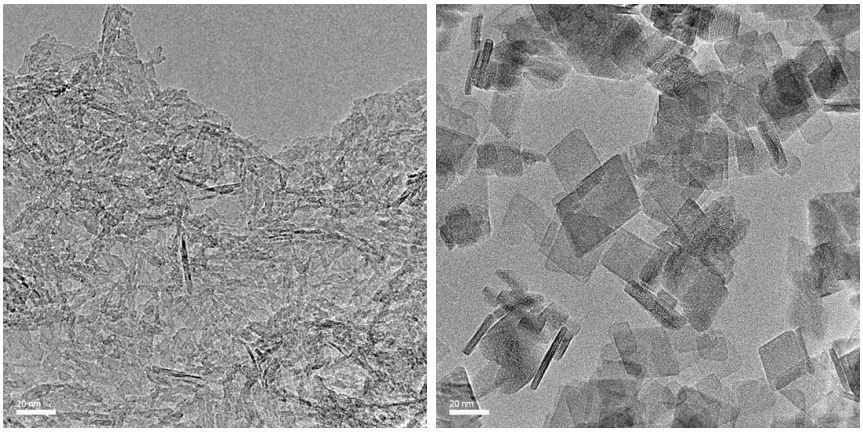

Figure 3.1 – TEM for boehmites Pural SB3 (on the left), and Disperal 40 (on the right).

The type of gas used (air or nitrogen) has different amounts of oxygen, that can lead to different oxygen defects on the samples synthesized. On the other hand, the water content in the gas (dry or 230 Pa) has the potential to create different defects and acid sites at the surface of the samples.

A classical methodology is applied to synthesize the samples of γ-alumina: the reaction takes place in a U-reactor, where 5 g of boehmite go through the following temperature program:

1. The temperature goes from 20 to 120°C at a constant rate of 5°C/min, and there is a 3h plateau whose aim is to remove most of the water;
2. The temperature goes from 120 to 650°C at the same constant rate, reaching a 6h plateau;
3. The temperature goes back to room temperature.

The different conditions for all γ-alumina samples synthesized are schematized in Figure 3.2 and summarized in Table 3.2.

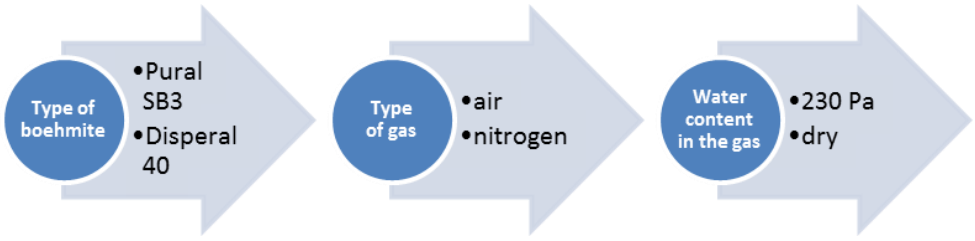

Figure 3.2 – Scheme for the synthesis conditions of γ-alumina.

Table 3.2 – Samples synthesized during this work and the corresponding synthesis conditions.

Sample #	Type of bohemite	Type of gas	Water content in the gas, Pp (Pa)
1	Pural SB3	air	230
2	Pural SB3	air	0
3	Pural SB3	nitrogen	230
4	Pural SB3	nitrogen	0
5	Disperal 40	air	230
6	Disperal 40	air	0
7	Disperal 40	nitrogen	230
8	Disperal 40	nitrogen	0

It is worth noting the difference in color obtained for the samples synthesized under air and nitrogen: the former are white powders, while the latter are gray powders with diverse tones.

3.2. Characterization techniques

Different and complementary methods are used in this work to characterize as well as possible all the samples obtained:

- X-Ray diffraction (XRD) to identify the structure of the alumina and to characterize its morphology;
- Measurement of N_2 adsorption isotherms at 77 K to assess the specific surface areas of the γ-alumina samples synthesized;
- Infrared (IR) spectroscopy to identify the nature of the surface hydroxyls present in the different samples, which appear in the 3800-3500 cm^{-1} zone, as well as their chemical environment (the coordination of the neighboring aluminum atoms). Depending on the morphology, it is expected there will be peaks with different intensities related to the intensity of each crystallographic face;
- Nuclear magnetic resonance (NMR) spectroscopy to study the nature and chemical environment of the surface hydroxyls present in the γ-alumina samples synthesized;
- Ultraviolet-visible (UV-Vis) to identify the amount and type of defects found in the different samples.

3.2.1. X-Ray diffraction (XRD)

X-ray diffraction (XRD) relies on the dual wave/particle nature of X-rays to obtain information about the structure of crystalline materials. The dominant effect that occurs when an incident beam of monochromatic X-rays interacts with a target material is scattering of those X-rays from atoms within the target material. The scattered X-rays undergo constructive and destructive interference in a process called diffraction.

A sufficiently crystallized material presents an atom arrangement according to crystallographic plans at a certain distance from each other. When X-ray beams with a certain wavelength get to that material, they are scattered in every direction (Figure 3.3), and the waves interfere constructively according to Bragg's law (3.1).

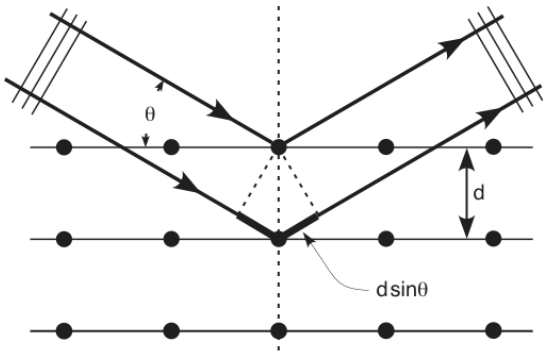

Figure 3.3 – X-ray beams being diffracted upon arrival at a certain material [39].

$$2d \sin\theta = n\lambda \tag{3.1}$$

Where:

d – Spacing between atom layers (nm);

Θ – Scattering angle;

n – Positive integer;

λ – Wavelength of the incident wave (nm).

Experimentally, a powder X-ray diffractometer consists of an X-ray source (usually an X-ray tube), a sample stage, a detector, and a way to vary the angle at which the X-ray is focused on, while the detector opposite the source reads the intensity of the X-ray it receives at 2θ away from the source path (Figure 3.4).

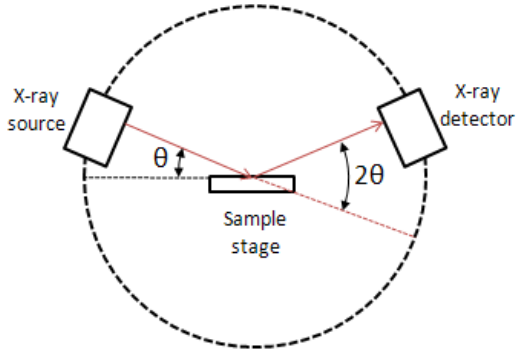

Figure 3.4 – Scheme of an X-ray diffractometer [39].

The position of the spectral lines obtained is characteristic of a structure, and the mid-length of the spectral lines is connected to the size of the particles analyzed according to Scherrer's law (3.2). In some cases, it is even possible to distinguish sizes in several directions.

$$L = \frac{K\lambda}{\beta \cos\theta} \tag{3.2}$$

Where:

L – Average crystallite size (nm);

K – Constant related to crystallite shape;

β – Peak width of the diffraction peak profile at half maximum height resulting from small crystallite size.

3.2.2. Nitrogen adsorption/desorption isotherms

The measurement of the nitrogen adsorption/desorption isotherm gives access to the pore volume, the pore distribution (using the Barrett, Joyner, and Teller – BJH – method), and the specific surface area (using the Brunauer, Emmett, and Teller – BET – theory) of materials. This is based on the measurement of the volume of adsorbed (or desorbed) gas at the surface of the material at a given temperature for different partial pressures of that gas. This method essentially characterizes the micro and mesoporosity, with the pores being sized between 2 and 50 nm.

This technique is often compared with the results of mercury porosimetry to estimate the macro or microporous nature of materials. If the BET surface is considerably higher than the mercury surface, the material has an important microporous nature. If, on the other hand, the BET surface is considerably

lower than the mercury surface, the material has an important macroporous nature. In this work, this method has not been applied because it is not adapted to powder.

3.2.3. Infrared spectroscopy (IR)

The range of the infrared (IR) region is 12800-10 cm^{-1} and it can be divided into near-infrared region (12800-4000 cm^{-1}), mid-infrared region (4000-200 cm^{-1}) and far-infrared region (50-1000 cm^{-1}). Infrared spectroscopy is the analysis of mid-infrared light interacting with a molecule, used to determine functional groups in molecules. Infrared light imposed on a molecule will not create electronic transitions, but it does contain enough energy to interact with a molecule causing vibrational and rotational changes. When the right energy is emitted by the source, it will be absorbed by the solid and the light observed will have a lower intensity comparing to that of the light exiting the source. The frequency of the band is characteristic of a function, and the intensity of the band or absorbance is correlated to the concentration of the function characterized. The absorbance corresponds to the ratio of the intensity observed to that emitted by the source and it is correlated to the concentration of the number of function analyzed thanks to the Beer-Lambert Law (3.3) :

$$A = \epsilon l C \tag{3.3}$$

Where:

A – Absorbance of the material;

ε – Molar attenuation coefficient of the material (m^2/mol);

l – Thickness of the material through which the light travels (m);

C – Molar concentration of the material (mol/m^3).

In general, the molar attenuation coefficients (ε) are not known, and this technique is only semi-quantitative.

Almost all IR spectrometers are Fourier-Transform IR spectrometers (FTIR). The device consists of a source, a Michelson interferometer, sample compartment, detector, amplifier, A/D convertor, and a computer (Figure 3.5). The source generates radiation which passes the sample through the interferometer and reaches the detector. Then the signal is amplified and converted to digital signal by the amplifier and analog-to-digital converter, respectively. Eventually, the signal is transferred to a computer in which Fourier transform is carried out.

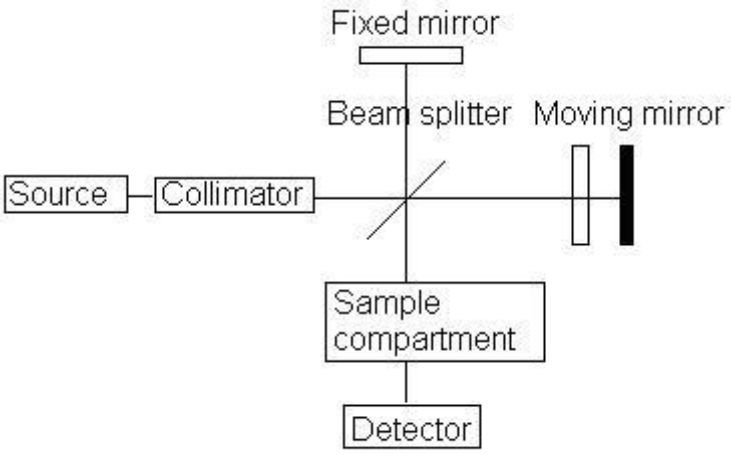

Figure 3.5 – Block diagram of an FTIR spectrometer [40].

For this work, there is a focus on the OH vibrational zone of the IR spectrum, that is to say between 3800 and 3500 cm^{-1}. Since the molar attenuation coefficients that are different for each type of hydroxyl are not known, the spectra will only be interpreted in a qualitative way.

3.2.4. Nuclear magnetic resonance spectroscopy (NMR)

Nuclear magnetic resonance (NMR) uses a large magnet to probe the intrinsic spin properties of atomic nuclei, using a component of electromagnetic radiation (radio frequency waves) to promote transitions between nuclear energy levels. When in the presence of a magnetic field, the nuclei present in the sample are characterized by a magnetic moment (3.4). The spins orient themselves in a parallel or anti-parallel configuration.

$$\mu = \gamma I \tag{3.4}$$

Where:

μ – Magnetic moment;

γ – Gyromagnetic ratio specific for a nucleus;

I – Angular momentum.

Under the effect of a magnetic field, the nuclei gain a rotation movement about the axis of the magnetic field, in a phenomenon called Larmor precession. The rotation frequency about the axis of the magnetic field, the Larmor frequency, is specific to each nucleus and depends on the magnetic field. This Larmor frequency is what allows the NMR experiments to be selective and specific to each atom. In practice, the selection of the frequencies observed is carried out by focusing the frequency of the bandwidth.

The magnetic field influences also the electronic cloud of the atoms that is perturbed and gives way to an induced magnetic field. Therefore, the magnetic field that is, in fact, felt by the atoms is the sum of the main and induced magnetic fields. This perturbation of the electronic cloud is also called screen effect and is directly related to the local environment (electronic and chemical) of the observed nucleus and gives way to the coordination of the nucleus and the nature of its neighbors. Ultimately, this leads to a modification of the resonance frequencies of the observed atoms with respect to the Larmor

frequency, in a phenomenon called chemical shift (3.5). In practice, the chemical shift is compared to the frequency of a reference compound.

$$\delta = \frac{\nu - \nu_{ref}}{\nu_{ref}} \tag{3.5}$$

Where:

δ – Chemical shift (ppm);

ν – Absolute resonance frequency of the sample (Hz);

ν_{ref} – Absolute resonance frequency of a standard reference compound, measured in the same applied magnetic field (MHz).

In straightforward terms, an NMR spectrometer consists on the following components: an intense, homogeneous and stable magnetic field; a probe which enables the coils used to excite and detect the signal to be places close to the sample; a high-power RF transmitter capable of delivering short pulses; a sensitive receiver to amplify the NMR signals; a digitizer to convert the NMR signals into a form that can be stored in computer memory; a pulse programmer to produce precise time pulses and delays; and a computer to control and process the data. A simple scheme of an NMR spectrometer can be found in Figure 3.6.

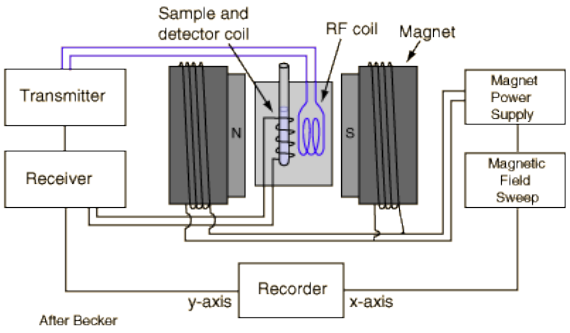

Figure 3.6 – Scheme of an NMR spectrometer [41].

This technique, which is a bulk analysis, allows the characterization of the environment of the analyzed atom. In this study, a proton (^{1}H) NMR is used, where an interpulse delay allows the spin system to relax toward an equilibrium, followed by a read pulse, and the acquisition time (Figure 3.7).

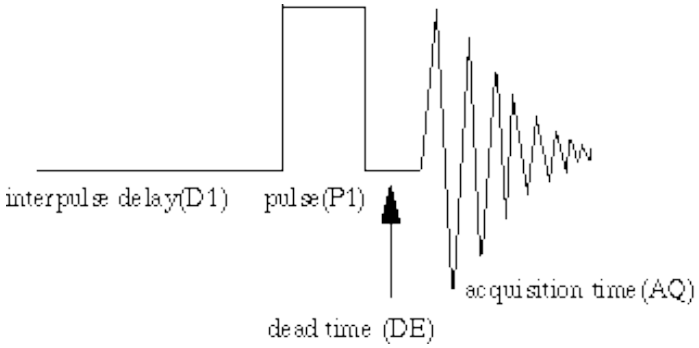

Figure 3.7 – Pulse sequence [42].

3.2.5. Ultraviolet-visible absorption spectroscopy (UV-Vis)

The energy radiation in the UV (200-400 nm) and visible (400-700 nm) range of the electromagnetic spectrum causes many molecules to undergo electronic transitions, that is, the energy from UV or visible light is absorbed by the molecule, making one of its electrons jump from a lower energy to a higher energy molecular orbital. As for the IR spectroscopy, the ratio between the intensity detected to the emitted intensity by the source is called absorbance and follows the Beer-Lambert Law.

In conventional spectrometers (Figure 3.8), the electromagnetic radiation is passed through the sample which is held in a small square-section cell. Radiation across the whole of the ultraviolet/visible range is scanned over a period of approximately 30 s, and radiation of the same frequency and intensity is simultaneously passed through a reference cell containing only the solvent. Photocells then detect the radiation transmitted and the spectrometer records the absorption by comparing the difference between the intensity of the radiation passing through the sample and the reference cells.

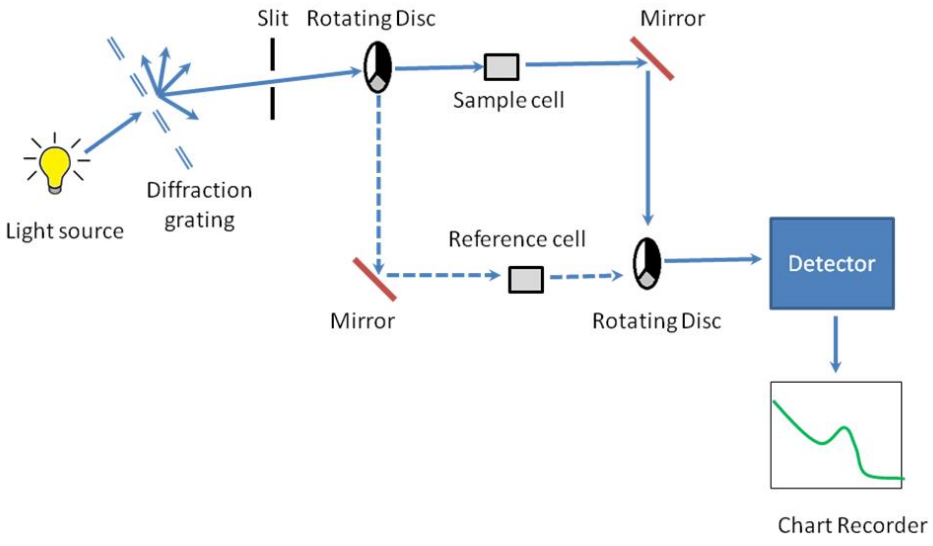

Figure 3.8 – Schematic figure for a UV-Vis spectrophotometer [43].

This kind of technique can detect transition metals, conjugated organic compounds, and also defects such as oxygen vacancies. These last ones are those that will be characterized in this study.

3.3. Thermogravimetry

3.3.1. General considerations

Thermogravimetry is a common technique that consists on measuring the mass variation of a sample following a certain temperature profile at a given controlled atmosphere, and relating that variation with, for instance, the adsorption or desorption of components found in the gas. In the course of this work, a thermobalance (*Thermobalance Setaram TAG-B12*) is used to determine the adsorption and desorption isobars of water and hydrocarbons on differently synthesized γ-aluminas.

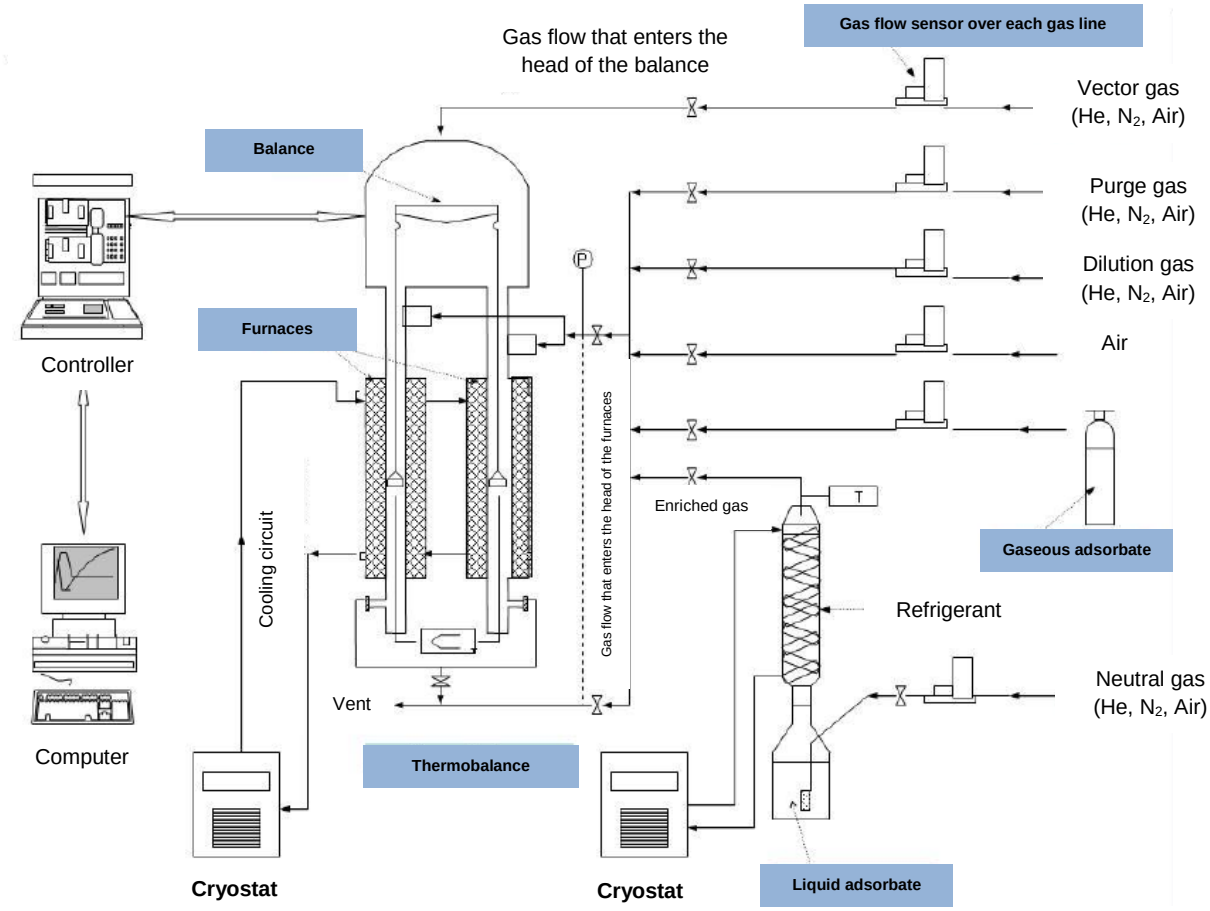

Figure 3.9 – Scheme of the thermobalance [44].

The scheme for the thermobalance used in this work is in Figure 3.9. It works from ambient temperature to 1200°C, being able to cover sample masses from some mg to 100 mg with a resolution of 1 μg, heating between 1-20°C with a total gas flow between 1-2 NL/h. It is a symmetric balance, since it has two furnaces regulated at the same temperature, inside which circulates the sweep gas at a known flow rate. This configuration strongly minimizes the phenomena of thermal drift between the furnaces and limits the mass corrections needed.

All the programming of the experiments, which includes, for instance, the heating rates, and the temperature steps, is given by a software called Calisto, developed by Setaram Society and ATKS.

The raw data obtained can be exported to Excel at the end of the experiment, and the parameters obtained this way are the time (t), the furnace temperature (T), and the mass (Tg).

3.3.2. Detailed description of the thermobalance

This thermobalance is composed by the following elements:

- **Furnaces**: The two furnaces are cylindrical, and it is possible to work until 1200°C. The temperature of each furnace is measured by a thermocouple inside it, under the baskets of measurement and reference. A controller allows the regulation of the temperature of the two furnaces according to the program defined by the user.

  A jacketing made of quartz is placed in the interior of each furnace, protecting them from aggressive gases. A side stitching at the top of the furnaces allows the introduction of reactive gases or gases loaded with adsorbate vapors, and there is also a connection with the head of the balance, that is always being swept by an inert gas.

  A micrometer screw placed on the output lines of the furnaces allows fine tuning of the gas flow rates passing through each of the furnaces in order to stabilize the baseline.

  A thermostatic bath, regulated at 18°C, isolates thermically the furnaces. The circulation of water in a double sealed casing prevents also heat transfer to the balance. The admission of water is done at the lower part of the furnace. A flow rate of 2 L/min is necessary and sufficient to assure good cooling. Stopping the water flow automatically stops the experiment;
- **Microbalance**: It is electronic. The scale of the balance is kept horizontal thanks to an electromagnetic system. In each extremity there is a basket, one for measurement, and another one for the reference, with a system of hooks that suspends them and positions them at a certain height inside the furnaces. The difference in mass between the two baskets is detected thanks to a system of a light-emitting diode, with a small mass difference displacing a diaphragm placed in the way of the light. A current is then sent through a coil, compensating the deviation of the scale, putting it back to a horizontal position. The current intensity is proportional to the mass variation. The scheme of the head of the balance is in Figure 3.10;

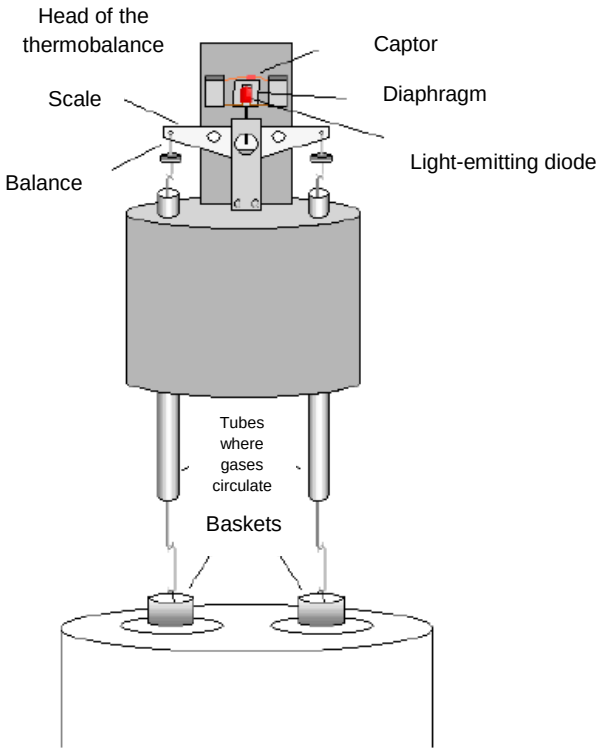

Figure 3.10 – Scheme of the head of the balance [44].

- **Gas circuits**: The experiments are done dynamically under the sweep gas at ambient pressure. The carrier gas used is helium, since it is easily purged when the atmosphere around the sample needs to be changed, and for its attractive characteristics: good thermal conductivity, low density, and low viscosity.

  A part of the inert gas is systematically sent to the head of the balance in order to protect the electronic and sensible parts. A lateral opening at the top of each furnace allows reactive or enriched gases to be sent to the balance without the risk of damaging the head of the balance. The gas delivered by the network must be pure and dry. It passes under filtering cartridges in order to perfect its quality.

  - **Gas lines**:

    Six gas lines supply the thermobalance:

    1. The “head” line is used to supply inert gas to the head of the balance in order to protect electronics from possible impurities;
    2. The “purge” line is used to supply neutral gas directly to the furnaces of the balance;
    3. The “saturator” line is used to supply vapor adsorbate to the balance, using a saturator system. This vapor is diluted in a neutral gas (a valve upstream of the saturator allows its isolation, if needed);
    4. The “bottle” line is used to supply a pure gas or a mixture of gases to the balance from a bottle, after being expanded to atmospheric pressure;
    5. The “air” line is used to do calcinations;
    6. The “purge” line is used to purge the system under a high flow rate of inert gas.

All the gases from the lines, except for the head of the balance, are directed to the laboratory vent during the purge phases, or are introduced to the thermobalance at the level of the furnaces.

To vary the composition of the gas entering the thermobalance, there are several options:

- Connecting a gas bottle with the right composition;
- Diluting a gas with an inert gas to decrease its concentration;
- Using a vapor enrichment system to increase the concentration of the gas. The determination of isotherms of various compounds on a given solid can be done by enriching the sweep gas with vapor adsorbate at a known concentration, circulating that enriched gas on the sample, and following the mass variation that brings about. This enrichment is accomplished by bubbling the gas, at a controlled flow rate, in the liquid (50 to 100 cm^3, typically), cooling the enriched gas by passing it through a condenser at a given temperature, and doing a secondary dilution if necessary (Figure 3.11).

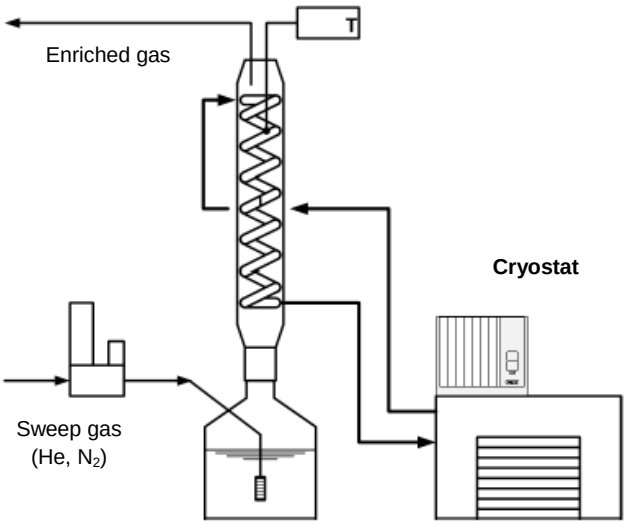

Figure 3.11 – Saturation system [44].

3.3.3. Experimental procedure

3.3.3.1. Water adsorption

For the desorption isobars of water on γ-alumina, a sample (~75 mg) is put in the thermobalance at a certain partial pressure of water (1, 20, 500, 1000 or 1400 Pa) with a nitrogen flow of 4 NL/h, being left to stabilize at room temperature until the local mass variation become negligible. A temperature program is then applied to the sample, going from 100 to 600°C in increments of 100°C (Figure 3.12). For each temperature, the sample is also left to stabilize until the local mass variation is insignificant.

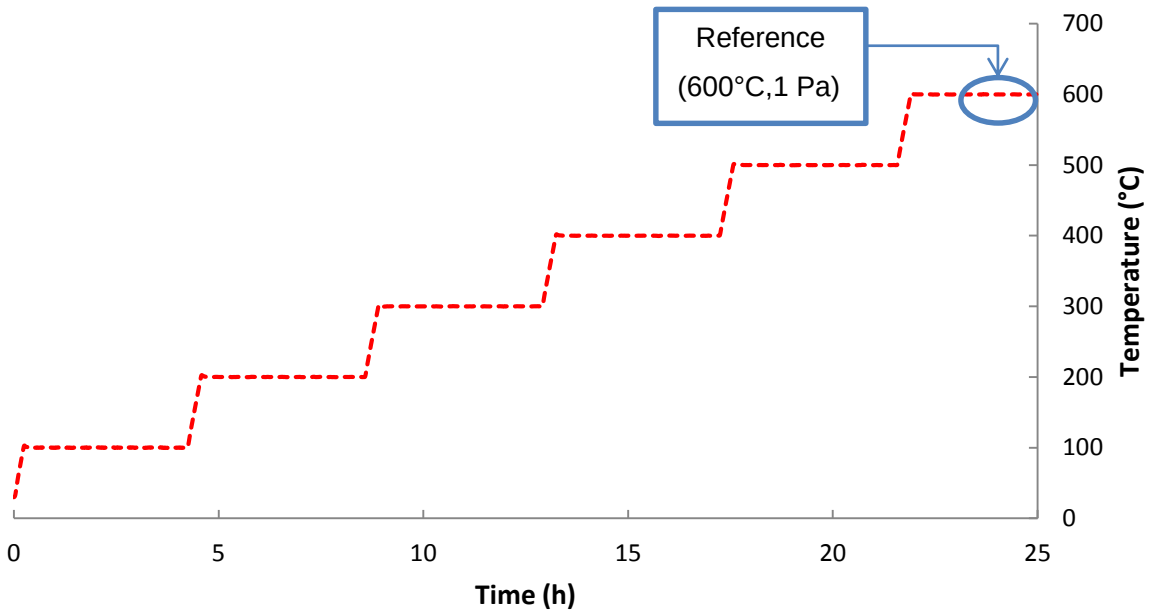

Figure 3.12 – Temperature program used for the desorption experiments.

For the adsorption isobars of water on γ-alumina, the methodology used is equal, except for the temperature program, which is reversed: it goes from 600 to 100°C in increments of 100°C (Figure 3.13.).

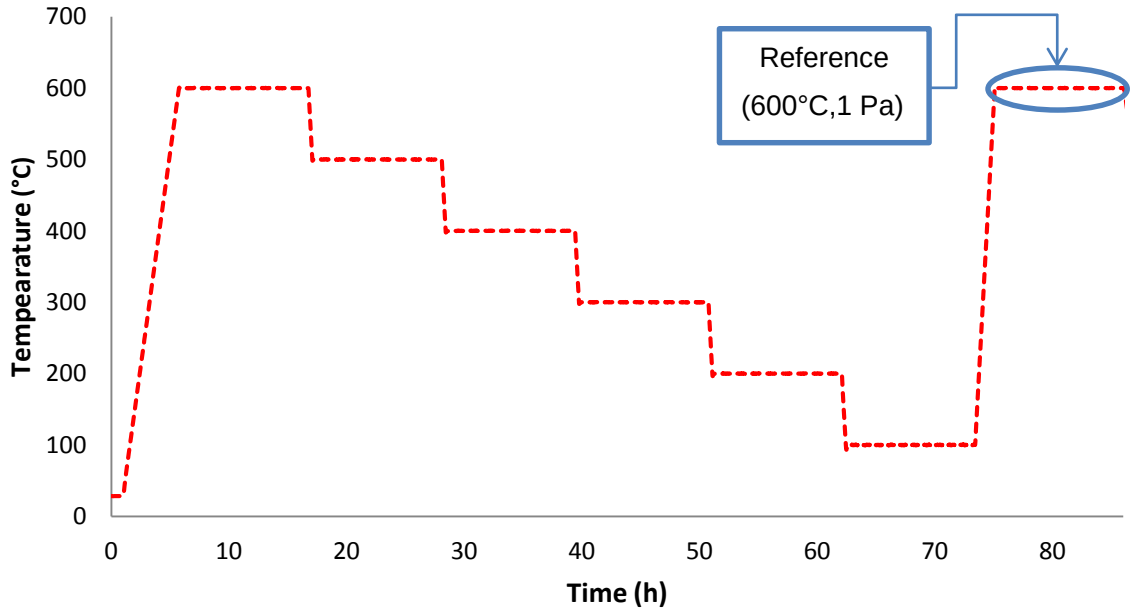

Figure 3.13 – Temperature program used for the adsorption experiments.

It is necessary to establish a relative reference to allow the correlation of adsorption and desorption results at different partial pressures of water. That reference is chosen at 600°C and 10 ppm of water; at these conditions, an approximation is made: the surface of γ-alumina does not present any hydroxyl groups. At this temperature, that is lower than the thermal decomposition temperature of boehmite to

obtain γ-alumina, it is assumed the sample is thermally stable. On the other hand, this partial pressure of water is the lowest one the thermobalance allows.

In order to obtain reproducible results, the stabilization time for the samples synthesized under air must be at least 2 h (after which the mass loss is 0,006 OH/nm^2/h) and for the ones synthesized under nitrogen at least 15 h (after which the mass loss is 0,03 OH/nm^2/h), as it can be seen in Figure 3.14. The duration of the plateaus is adjusted to ensure their stabilization.

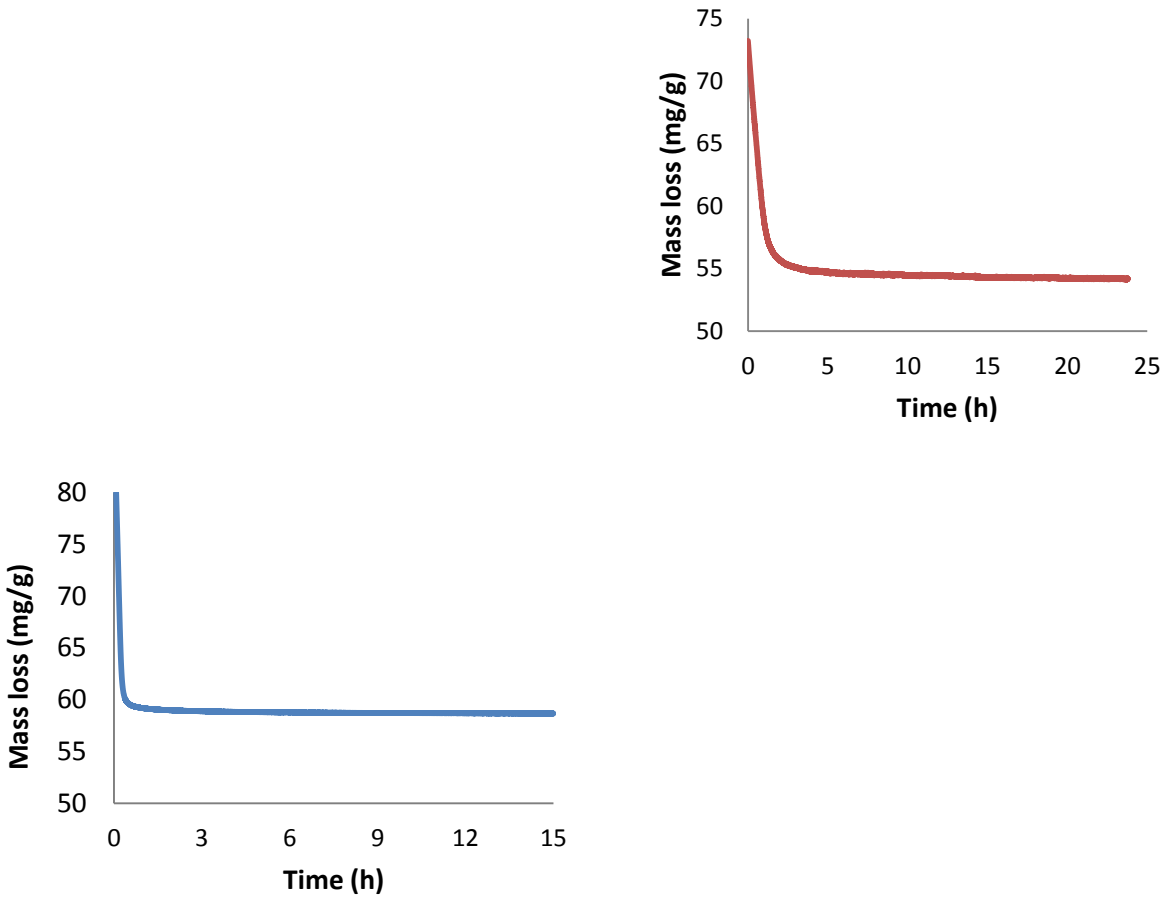

Figure 3.14 – Stabilization times for samples#1 and #3 at 30°C and a water partial pressure of 1 Pa.

In Figure 3.15, it is possible to see the mass variation with the temperature of sample #3 at a water partial pressure of 1400 Pa. To determine the number of surface hydroxyls, it is necessary to calculate the difference between the mass loss at the adsorption plateau and the reference plateau, which was chosen at a water partial pressure of 1 Pa and 600°C, where it is assumed the surface of the sample is devoid of hydroxyls.

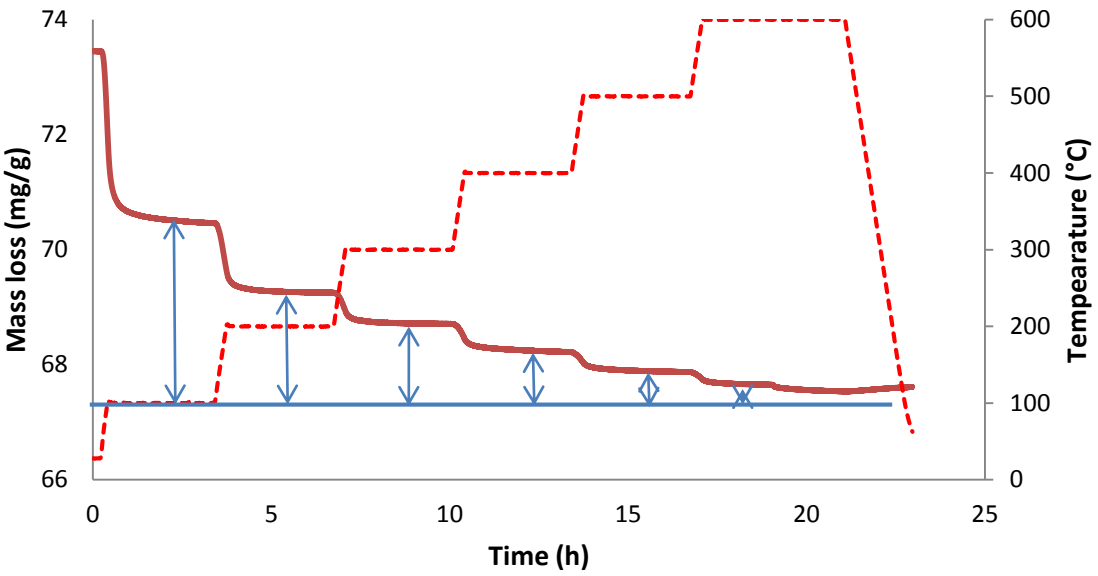

Figure 3.15 – Mass loss for sample #3 at a water partial pressure of 1400 Pa.

When the mass variation for different partial pressures of water and temperatures is known, it is possible to determine the number of hydroxyl groups at the surface of γ-alumina by applying (3.6). Therefore, the hydroxyl groups for different synthesis conditions are quantitatively obtained, and can be correlated to the quantity of hydrocarbons adsorbed.

$$OH/nm^2 = \frac{Dm \times N_A \times 2}{1000 \times M_{H_2O} \times S_{BET} \times 10^{18}} \tag{3.6}$$

Where:

Dm – Mass variation associated with water (mg/g);

N_A – Avogadro's number (6,02 x 10^{23} (1/mol);

2 – Water dissociates to form two hydroxyls;

M_{H2O} – Water molar mass (18 g/mol);

S_{BET} – Specific surface area of the sample (m^2/g).

3.3.3.2. Hydrocarbons adsorption

The protocol used to study the ethylene adsorption on γ-alumina is in Figure 3.16. An alumina sample is placed in the thermobalance (~ 60 mg) and put in equilibrium at the water partial pressure necessary to reach the hydroxylation rate wanted, under a nitrogen flow rate of 4 NL/h. The sample undergoes several activation-adsorption-desorption cycles:

- Activation at 100°C and stabilization during 2 h;
- Decrease of temperature till 30°C, followed by injection and adsorption of ethylene until the mass is stable;
- Desorption under nitrogen at 30°C;
- Activation at 200°C and stabilization during 2 h;
- etc. till 600°C.

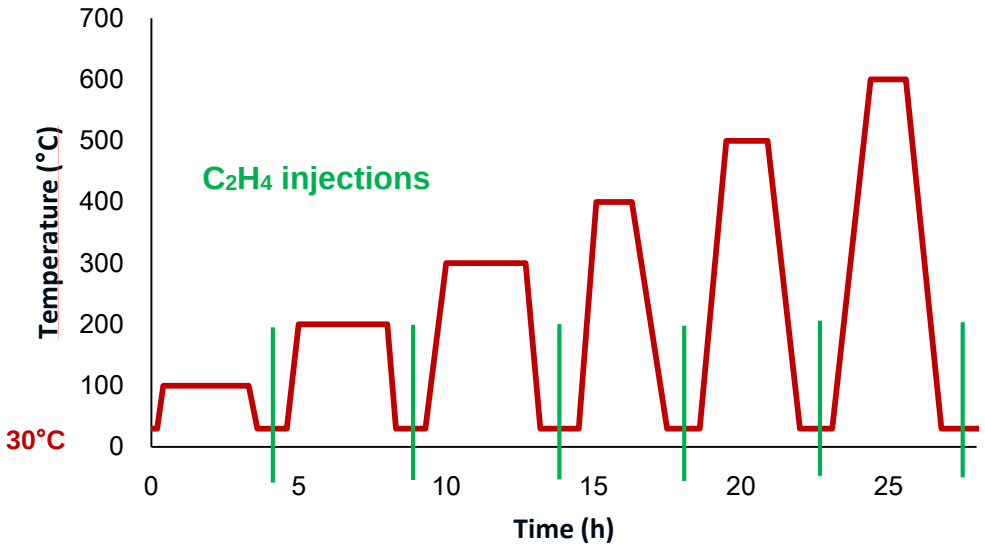

Figure 3.16 – Ethylene adsorption at fixed surface coverages.

These cycles have the advantage of greatly limiting rehydroxylation, ensuing precise results about the evolution of the behavior of the surface in function of the surface coverage. The alumina is reactivated in an atmosphere whose water content is controlled before each adsorption. Furthermore, the adsorption temperature is fixed at 30°C since it allows adsorption in great quantities, and the mass variations are then measured with more precision. Finally, the duration of the stabilization plateaus at different temperatures is minimized: the more temperature, the less time the mass needs to stabilize.

4. Results and discussion

4.1. Water adsorption/desorption on γ-alumina

4.1.1. Study of reference sample

The reference sample is synthesized by the thermal decomposition of Pural SB3 at 650°C for 6h under air with a water partial pressure of 230 Pa. The characteristics of the γ-alumina obtained are on Table 4.1, which include the size of its grains and the specific surface area. The corresponding XRD spectra (Figure 4.1) show that the alumina obtained is a γ-alumina, with coincident theoretical and experimental diffraction rays.

Table 4.1 – Most important characteristics of the reference sample.

Analysis	Results
XRD	Figure 4.1
SEM	5-80µm grains
Specific surface area, S_{BET} (m^2/g)	228
NMR ^{27}Al (Al^{VI}/Al^{IV})	74/26

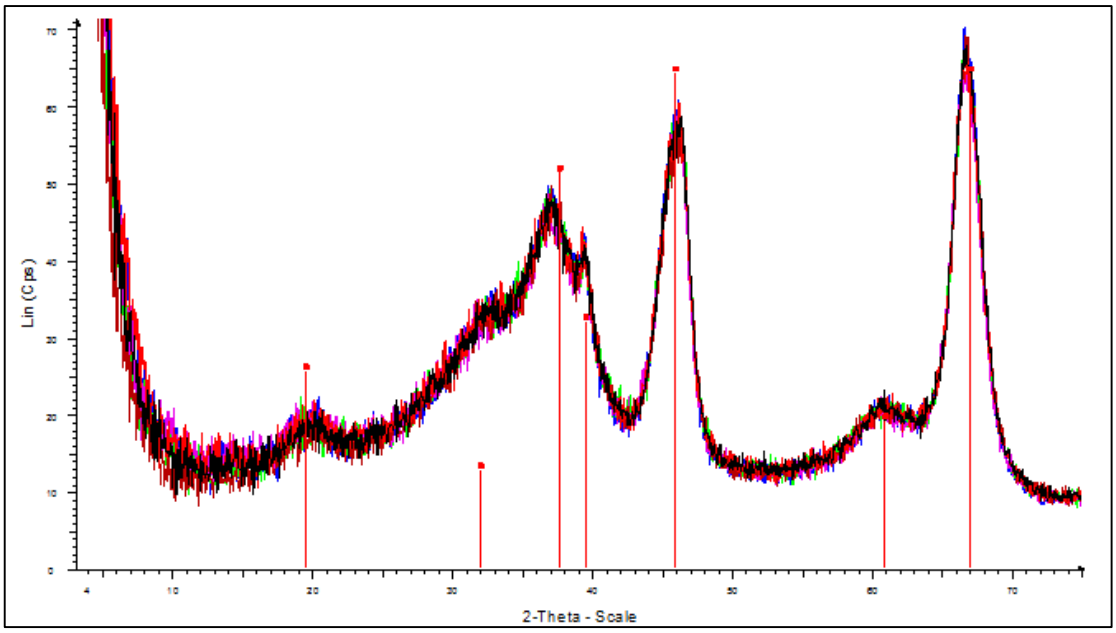

Figure 4.1 – XRD of the reference sample.

The water desorption measurements for the reference sample are obtained (Figure 4.2) for the water partial pressures of 1, 20, 500, 1000, and 1400 Pa, using as reference a plateau at 600°C at a water partial pressure of 1 Pa, where it is considered that the surface of the sample is completely dehydrated (no more hydroxyls). The numerical values obtained are reported in Table 4.1.

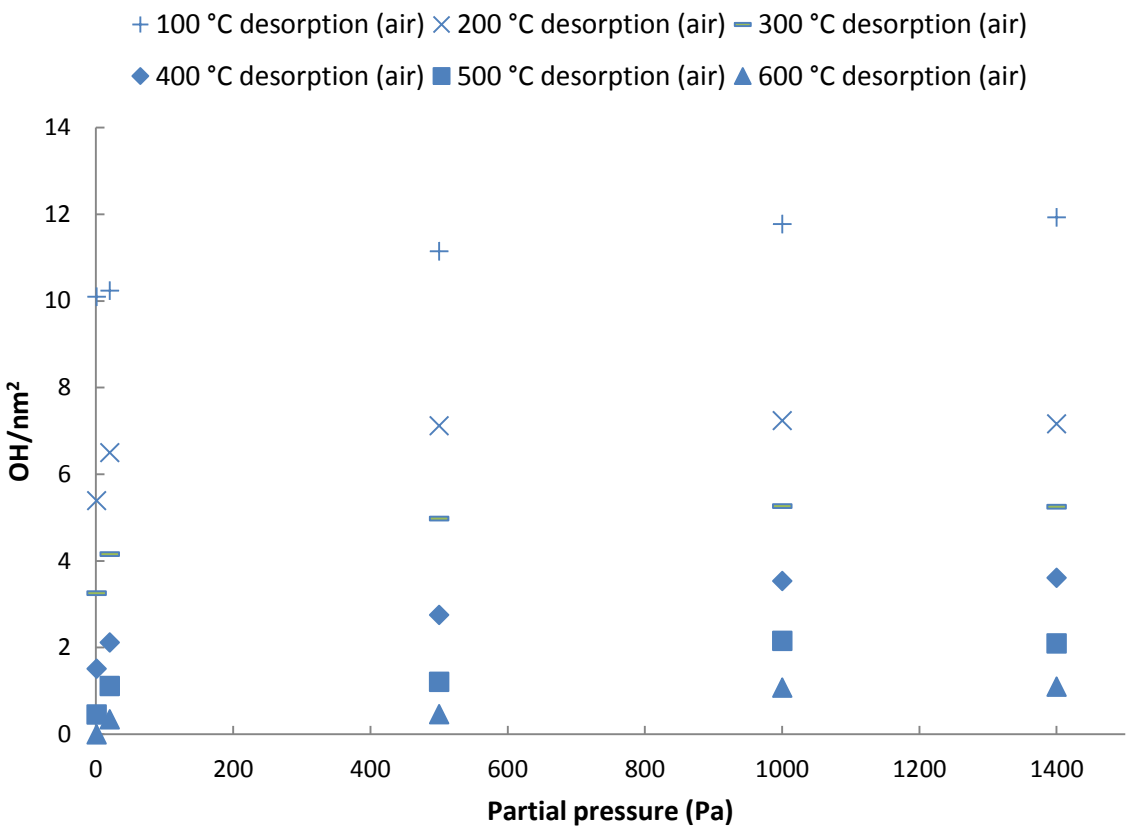

Figure 4.2 – Water desorption isotherms obtained for the reference sample.

Table 4.2 – Results for the water desorption isotherms obtained for the reference sample.

Water partial pressure, Pp (Pa)	100°C	200°C	300°C	400°C	500°C	600°C
1	10,10	5,40	3,26	1,51	0,46	0 (ref)
20	10,24	6,50	4,16	2,12	1,12	0,35
500	11,15	7,12	4,98	2,76	1,21	0,46
1000	11,78	7,24	5,27	3,54	2,16	1,08
1400	11,93	7,17	5,25	3,61	2,10	1,10

For low water partial pressures (1-20 Pa), the amount of surface hydroxyls increases linearly with a pronounced slope that depends on temperature, until, at high water partial pressures (500-1400 Pa), this amount reaches a plateau, also depending on temperature, with little change in the maximum values. Before going further in the interpretation, some points have to be verified.

To verify the thermic stability of the sample, the same desorption program is used with a key change: a pretreatment at a certain temperature (600 or 450°C) for 5 h precedes the usual temperature program (Figure 4.3).

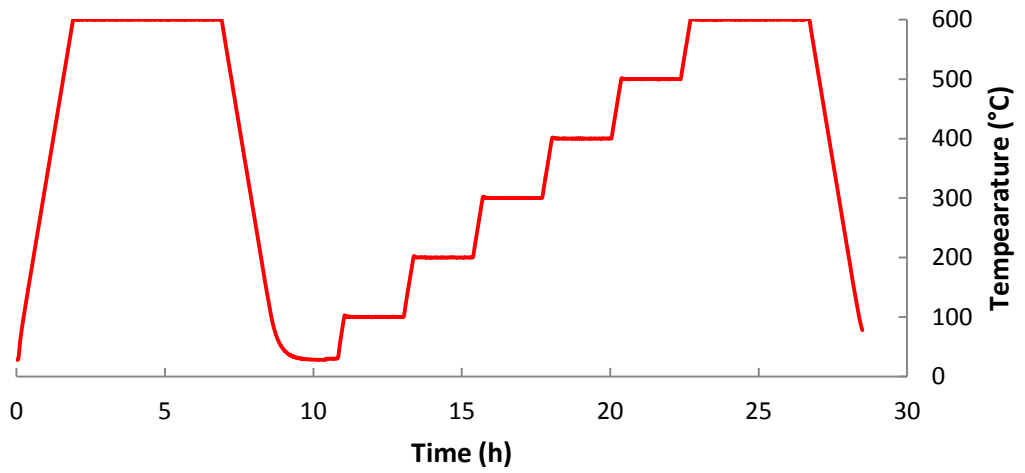

Figure 4.3 – Temperature programmed for a desorption isotherm, with a pretreatment step at 600°C.

The water desorption isobars for the reference sample preceded by a pretreatment step at 450 or 600°C are represented in Figure 4.4. It is possible to ascertain that the pretreatment step does not seem to heavily influence the water desorption on this sample, especially for higher temperatures.

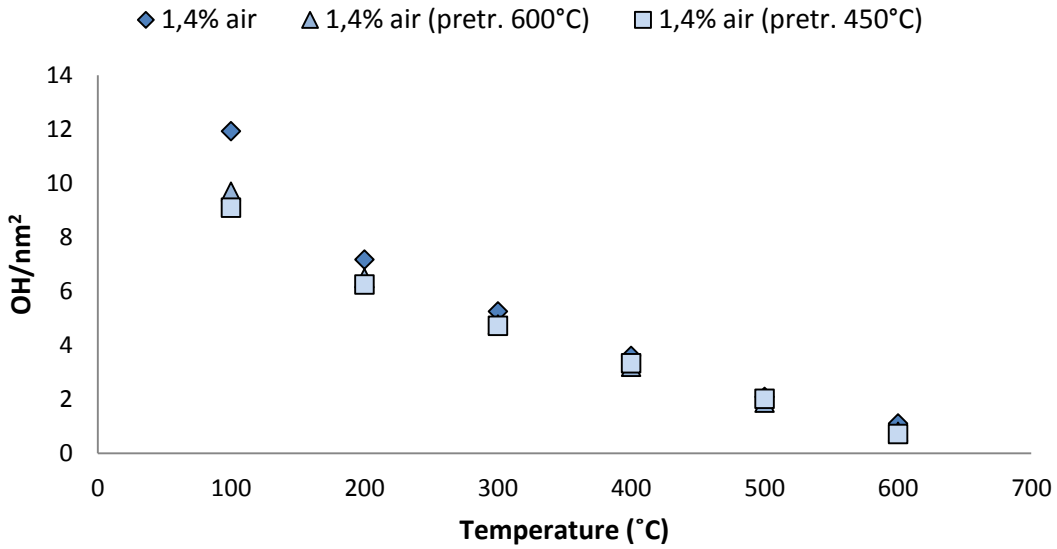

Figure 4.4 – Water desorption isobars at 1400 Pa of water with and without a pretreatment step.

To verify if the desorption isotherms correspond to equilibrium states, that is, if desorption and adsorption lead to the same surface coverage at the same temperature and water partial pressure, two experiments are carried out at 1400 Pa. The sample is first heated to 100 or 400°C, then heated to 600°C (hydroxyls are desorbed), and after that, cooled down again to 100 or 400°C (hydroxyls are readsorbed).

The applied temperature program is illustrated in Figure 4.5, showing the 400-600-400°C experiment.

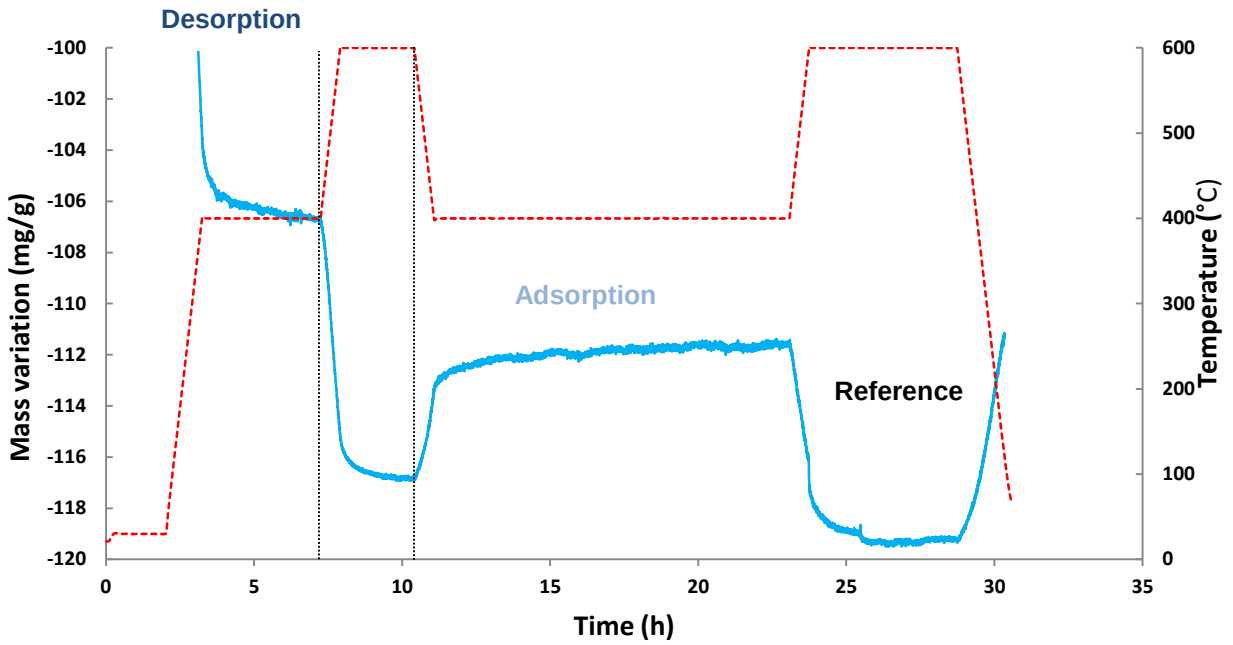

Figure 4.5 – Desorption to adsorption experiment at 400 and 600°C for the reference sample.

The values obtained for desorption and adsorption at the same temperature and water partial pressure (100 or 400°C and 1400 Pa, respectively) are not equivalent. Figure 4.6 puts in evidence the disparity between the surface coverage reached by desorption (3,63 OH/nm^2 at 400°C and 12,36 OH/nm^2 at 100°C) and adsorption (2,17 OH/nm^2 at 400°C and 7,80 OH/nm^2 at 100°C). The values differ by more or less 40%.

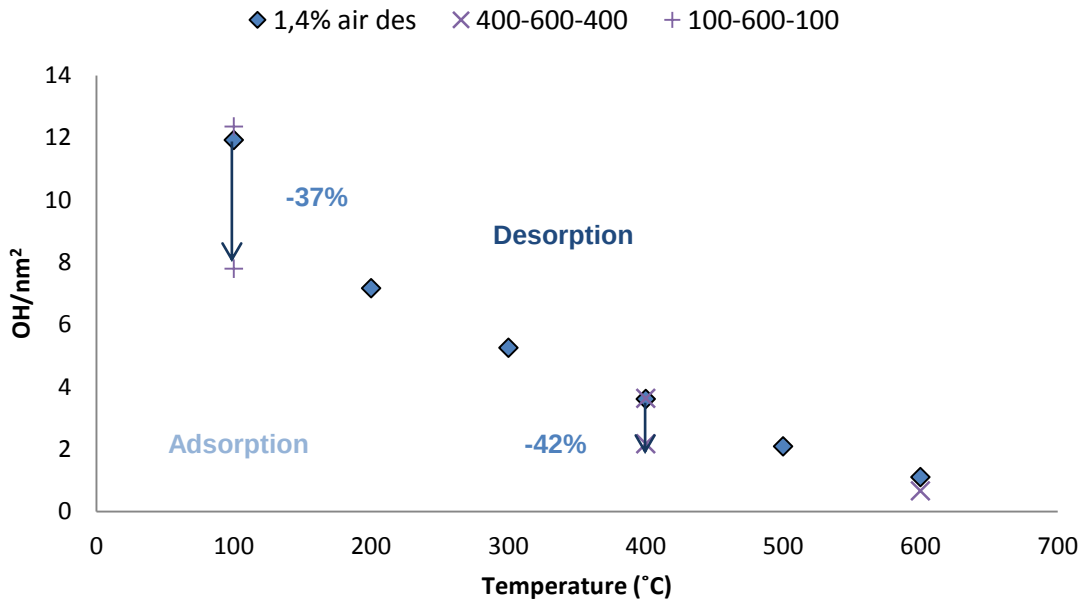

Figure 4.6 – Results for the 400-600-400°C and 100-600-100°C experiments, and comparison with the water desorption isobar at 1400 Pa.

This phenomenon is observed for all temperatures, as shown by the comparison between the points obtained by water desorption and adsorption in Figure 4.7.

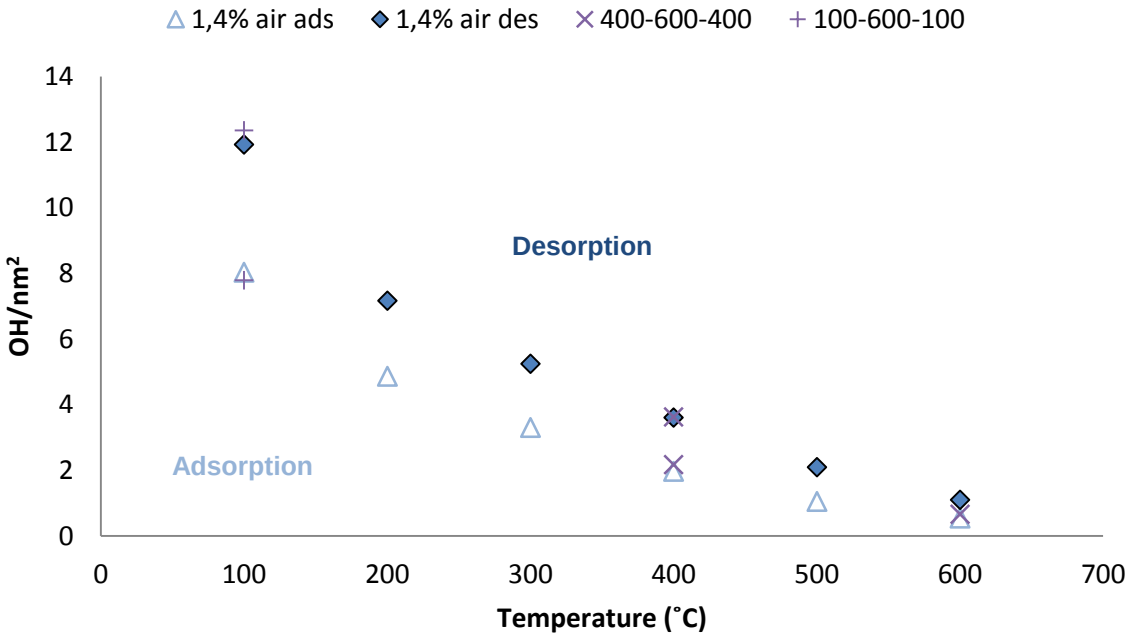

Figure 4.7 – Water desorption and adsorption isobars at 1400 Pa for the reference sample.

The points from the two return experiments, at 400-600-400°C and 100-600-100°C, are concordant with the values obtained from the complete experiments of progressive desorption or adsorption. On the other hand, two adsorption/desorption cycles are also run in order to check the reproducibility and reversibility of the adsorption and desorption measurements. From them, it is possible to conclude that the adsorption/desorption cycles are reproducible and reversible.

There are several hypotheses that could explain this disparity between the values obtained for adsorption and desorption.

The first hypothesis is that the surface structure changes; it could, for example, undergo sintering, which would be catalyzed by the presence of water [45]. Indeed, the first temperature in the adsorption program is 600°C, which is lower than the temperature of transition to δ-alumina, but close to the conditions of dealumination. However, since there is the same quantity adsorbed for the pretreated and the non-pretreated samples at 600°C, it seems that no sintering occurs at that temperature. This is also confirmed by a very low decrease of the specific surface area (from 228 to 207 m^2/g) after treatment at 600°C. Therefore, sintering is not a viable explanation for the difference between the adsorbed quantities reached by desorption and adsorption.

Then, the possibility of occurrence of capillary condensation is studied, in which case a hysteresis loop would appear. To study this hypothesis, the Kelvin equation (4.1) is applied to this system from 20 to 300°C at a water partial pressure of 1400 Pa. The values for the surface tension of water are from reference [46].

$$ln\frac{p}{p^0} = \frac{2\gamma V_m}{rRT} \quad (4.1)$$

Where:

p – Vapor pressure (Pa);

p_0 – Saturation vapor pressure (Pa);

γ – Surface tension (J/m^2);

V_m – Molar volume of the liquid (m^3/mol);

r – Radius of the droplet (m).

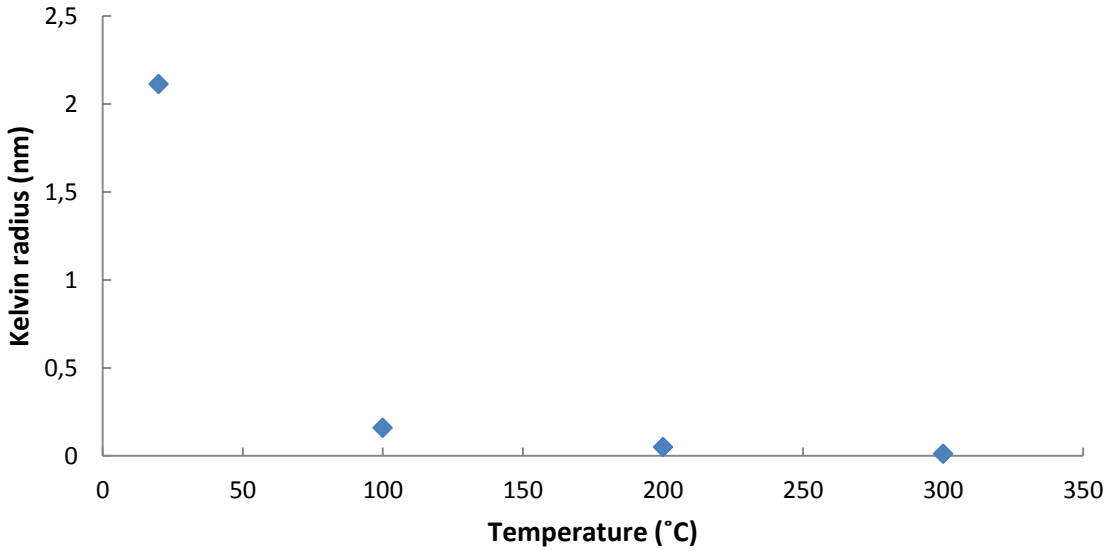

Figure 4.8 – Kelvin radii for the reference sample from 20 to 300°C at 1400 Pa.

The Kelvin radii obtained in function of the temperature are drawn in Figure 4.8. For temperatures higher than 100°C, capillary condensation does not occur in the pores of this sample. As such, this is not a viable explanation for the different adsorbed quantity from adsorption and desorption experiment.

Finally, it is considered that the measurements obtained by desorption cannot correspond to equilibrium points. This implies that some hydroxyls are very difficult to desorb, that is to say their desorption activation energy is very high and far higher than that of adsorption. In that case, desorption would be a slower phenomenon than adsorption, and a very long time would be needed to reach the equilibrium. Moreover, the probability of two hydroxyls meeting to form water gets lower the longer the sample is dehydrated; this could also influence the slowing down of desorption. To verify this hypothesis, it is necessary to extract the desorption activation energy from the experimental data.

Dima and Rees [47] have developed an equation which establishes a relationship between the desorption activation energy and the surface coverage, using the data from a water desorption isobar. For that, the authors considered that desorption is a first-order reaction, and that there is no readsorption during desorption.

For the desorption reaction A ⇄ A*, the desorption rate is given by (4.2).

$$\frac{d[A*]}{dt} = k_d[A*] - k_a[A] \tag{4.2}$$

Where:

[] – Concentration of the species (mol/m^3);

$k_{a,d}$ – Reaction rate constant for adsorption and desorption, respectively (s^{-1});

t – Time (s).

Considering the readsorption rate equal to zero, it is possible to obtain (4.3), where the rate constant is given by (4.4).

$$\frac{d\theta}{dt} = k_d\theta \tag{4.3}$$

$$k_d = A_d e^{-\frac{E_{a,d}}{RT}} \tag{4.4}$$

Where:

$k_{a,d}$ – Reaction rate constant for desorption (s^{-1});

Θ – Surface coverage (g/g);

A_d – Pre-exponential factor for desorption (s^{-1});

$E_{a,d}$ – Activation energy for desorption (kJ/mol).

After some mathematical treatment, the authors obtain equation (4.5), where the function p is given by (4.6).

$$\frac{\sum_i ln\theta_i \cdot p\left(\frac{E}{RT_i}\right)\sum_i p\left(\frac{E}{RT_i}\right)T_i e^{-E/RT_i}}{\sum_i p^2\left(\frac{E}{RT_i}\right)} - \sum_i ln\theta_i T_i e^{-E/RT_i} = 0 \tag{4.5}$$

$$p(x) = \frac{\exp(-x)}{x} + \int_x^\infty \frac{\exp(-u)}{u}\,du \tag{4.6}$$

This equation is applied to the values obtained for the desorption experiments at 1, 20, 500, and 1400 Pa. After a numerical approximation of function p, the results are reported in Figure 4.9. The points obtained by Hendrisken *et al.* [48] result from the measurement of the heat of adsorption by calorimetry, and are used as the first values for Solver.

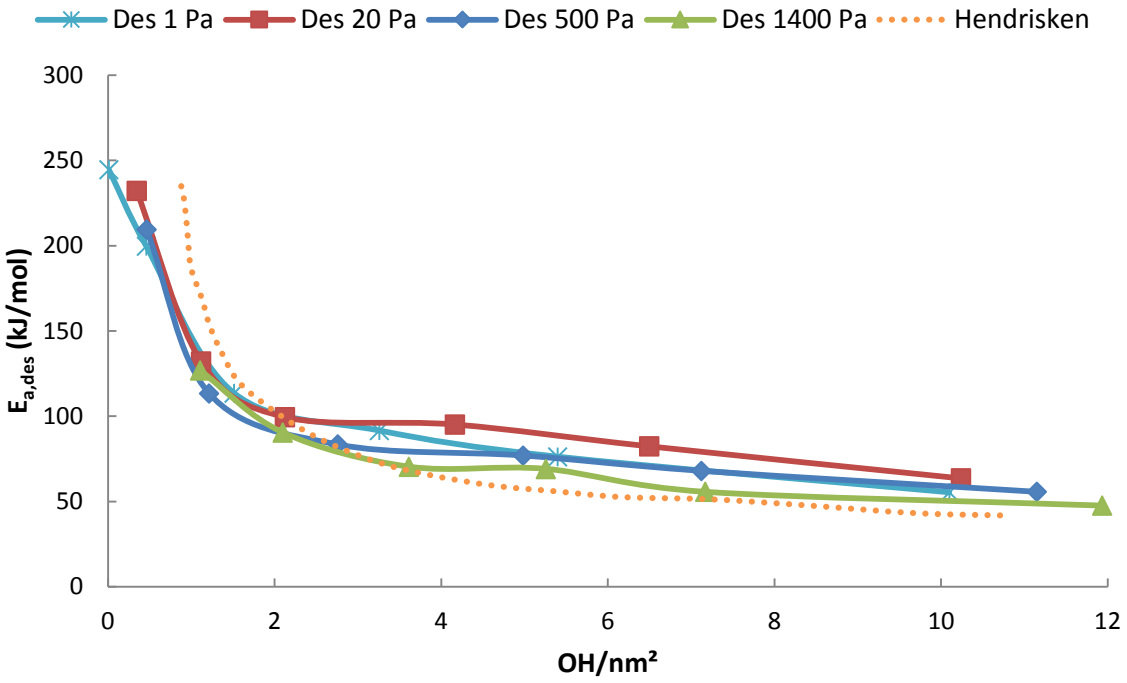

Figure 4.9 – Influence of the surface coverage on the desorption activation energy of the reference sample.

Calculations of desorption activation energy in function of surface coverage by hydroxyl lead to curves close to the experimental points of Hendrisken. Thus, they can be considered as quite accurate ones.

These curves show that the desorption activation energy depends on the surface coverage whatever the water partial pressure, becoming particularly high for the almost dehydrated surface. This confirms that the surface of the alumina is heterogeneous with different types of adsorption sites. For high surface coverage, the activation energy is close to the vaporization enthalpy of water (40,7 kJ/mol at 100°C [49]), but for low surface coverage, it becomes very high (> 100 kJ/mol). Thus, the last hydroxyls are very difficult to desorb, and as such, it is probably difficult to reach an equilibrium by desorption. This activation energy seems to be independent from the water partial pressure, since all the curves tend to the same one, considering there was an approximation made.

To try to determine if these remaining hydroxyls can be associated with one or several specific types of hydroxyls, the sample is heated at different temperatures and characterized by IR spectroscopy. It is submitted to the same temperature program used to verify the equilibrium, that is, two 400°C plateaus separated by a 600°C plateau. However, the water partial pressure is 20 Pa due to technical constraints. The spectra obtained are drawn in Figure 4.10: the red line corresponds to the spectrum of the solid heated to a 400°C plateau, after desorption of some water molecules, and the blue line to the one of the previous solid heated to 600°C and back to 400°C, after adsorption of water.

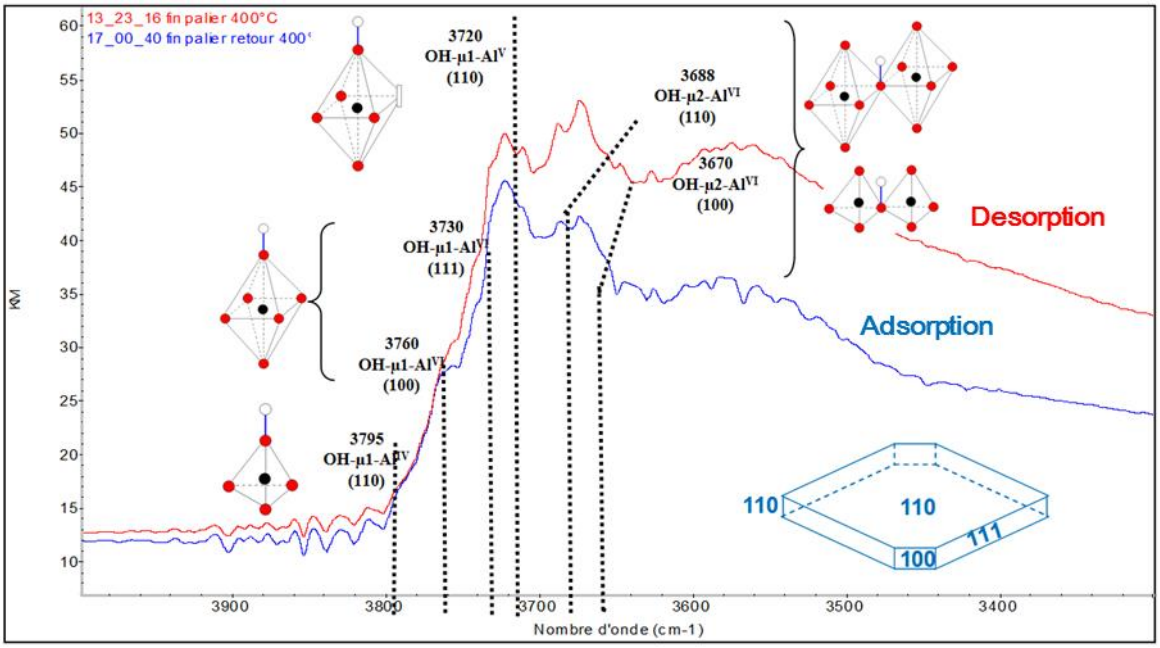

Figure 4.10 – IR analysis of a 400-600-400°C experiment at 20 Pa for the reference sample after desorption from ambient to 400°C (red line) and after the 400-600-400°C temperature program (blue line)

The quantities of types of hydroxyls in the two 400°C plateaus are different, which confirms that some hydroxyls are non-desorbed by performing desorption. Indeed, several bands are lower in the second spectrum. However, the variation of the bands ratio cannot be interpreted, because each hydroxyl type has probably its specific molar attenuation coefficient, which is temperature-dependent, and these coefficients are unknown.

To get more quantitative information, a H^1 NMR analysis is performed in a similar way to the IR study. In Figure 4.11, the blue line corresponds to the spectrum of the solid at the end of the first 400°C plateau (after desorption of water from ambient temperature), while the red line corresponds to the spectrum of the solid at the end of the last 400°C plateau (after adsorption of water from 600°C). The gray one corresponds to the spectrum obtained by subtracting the two previous ones.

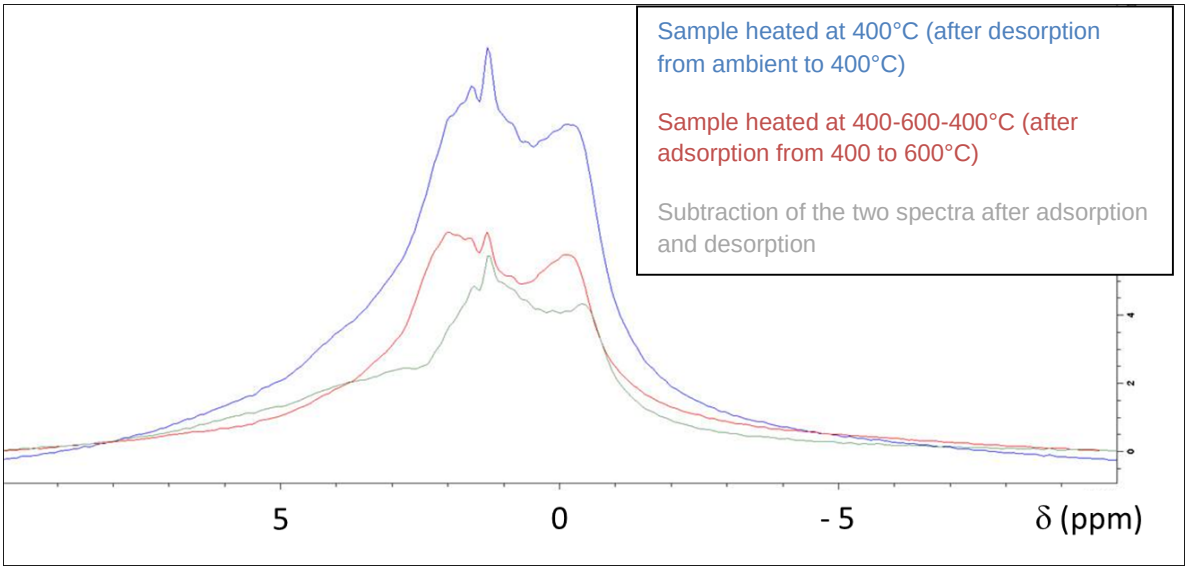

Figure 4.11 – H^1 NMR spectra for the 400-600-400°C experiment for the reference sample (red line for the spectrum of the solid after adsorption, and blue line for the spectrum of the solid after desorption).

Taoufik *et al.* [50] suggest some attributions to the peaks, in particular that the ones with negative chemical shifts correspond to terminal hydroxyls, while the ones with positive chemical shifts correspond to bridged/tribridged hydroxyls.

In accordance with the IR spectra following the same temperature program, the NMR spectra show that the quantities of hydroxyls in the two plateaus are different (lower for the sample after adsorption from 600 to 400°C), but the ratios between the different types of hydroxyls seem to be maintained. This indicates that there are always at least two different types of hydroxyls desorbed at the same time, as is the case where to desorb a water molecule, a terminal hydroxyl has to combine itself with a hydrogen from another hydroxyl. The latter is more probably a bridged or tribridged hydroxyl, so that after the hydrogen departure, the oxygen will still have a correct coordination number. Consequently, it is not possible to attribute a specific type of hydroxyl to the ones that have difficulty desorbing: in other words, the remaining hardly desorbed hydroxyls can be any type of hydroxyl, but probably with different probabilities depending on the family.

The adsorption isotherms obtained through adsorption experiments are shown in Figure 4.12. These isotherms do not tend to the same plateau, and as such, there are different adsorption sites involved in the adsorption phenomenon, which is in agreement with previous results. The points at high partial pressures and low temperatures seem higher than expected, but this could be due to the fact that there is physisorption happening at these conditions, making the stabilization difficult.

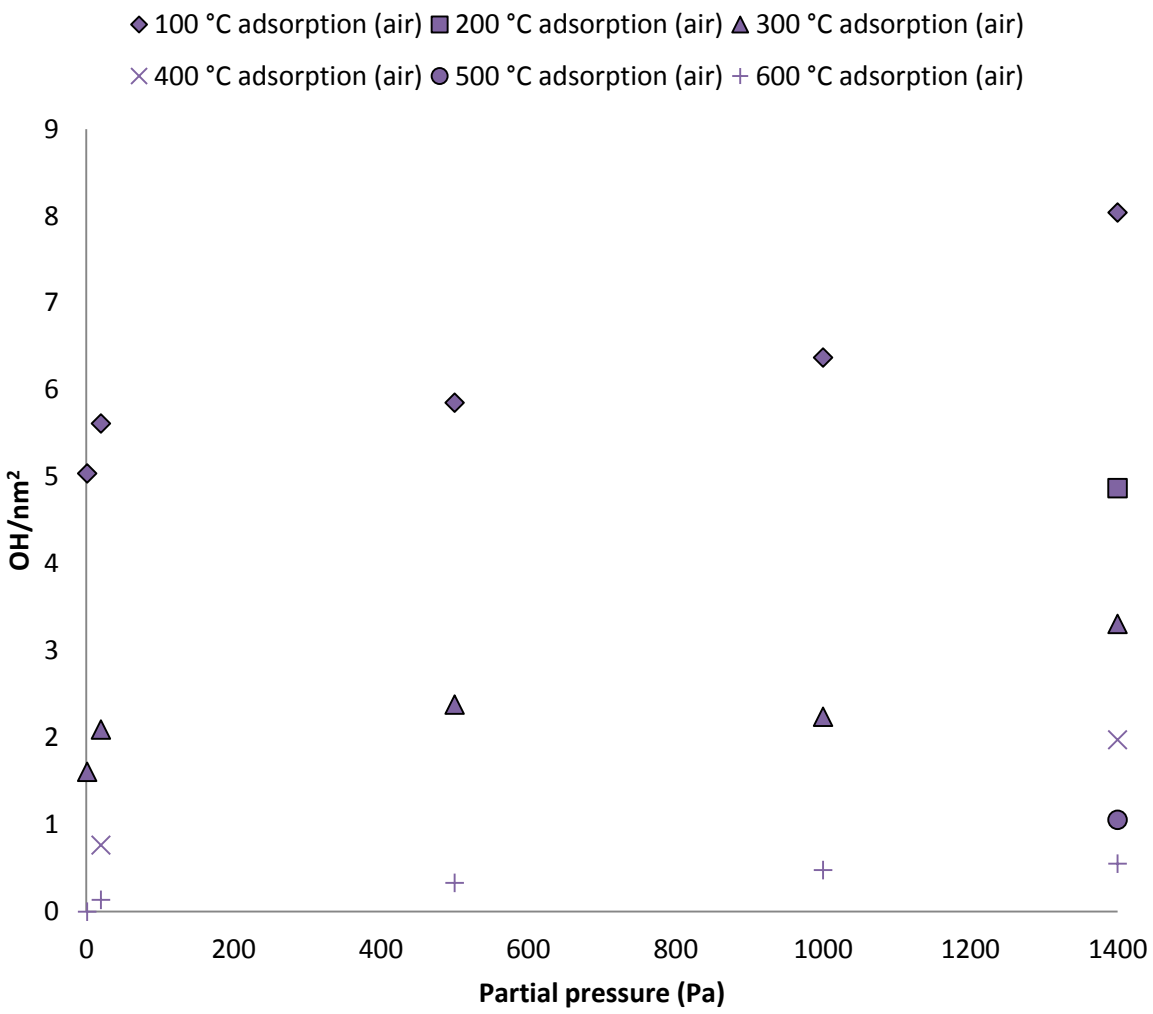

Figure 4.12 – Water adsorption and desorption isotherms for sample #1.

To simulate the adsorption points, it is necessary to use adsorption models. Since there are many adsorption sites involved, the models that can be used are, for instance:

- based on Density Functional Theory (DFT);
- Langmuir multisite;
- Statistical models.

Starting with Density Functional Theory, quantum chemistry calculations are performed [51,52] on periodic models depicting the system as a unit cell repeated along the 3 directions of space [53], with the VASP code [54,55]. Alumina surface models for the γ-alumina (100) and (110) orientations are adapted from Digne *et al.* [56,57] and Wischert *et al.* [58] and reoptimized at a up-to-date level of theory (GGA functional *plus* dispersion corrections). [59] Adsorption energy of water for growing water coverage are estimated, taking into account possible dissociation of the water molecule into hydroxyl groups. Analysis of surface vibrational modes enables the quantification of approximate enthalpic and entropic terms (harmonic approximation), leading to the estimation of adsorption enthalpy and Gibbs

free energy at the desired temperature and water partial pressure, assuming an ideal gas behavior for gaseous water [60].

The curve that is obtained based on DFT can be seen in Figure 4.13 in comparison with the adsorption experimental points at a water partial pressure of 1400 Pa. The tendency of the curve and the experimental points is similar, although there is a gap between the values themselves. This can be linked to a problem of the definition of the reference state. In this study, at a water partial pressure of 1 Pa and 600°C, the surface of γ-alumina is considered completely dehydrated. Yet, there will be always some hydroxyls at the surface at these conditions, which are considered in the simulated model. Consequently, a correction is applied to the experimental points that improve the correspondence between experiments and calculations, but a difference is maintained. This point will have to be investigated. However, the difference seen at 100°C is probably because the simulated model does not take into consideration the physisorption phenomenon, which happens more strongly at this temperature, contrary to the experiments. As such, this model fits the adsorption experimental values for this sample in a satisfactory, if lacking, way.

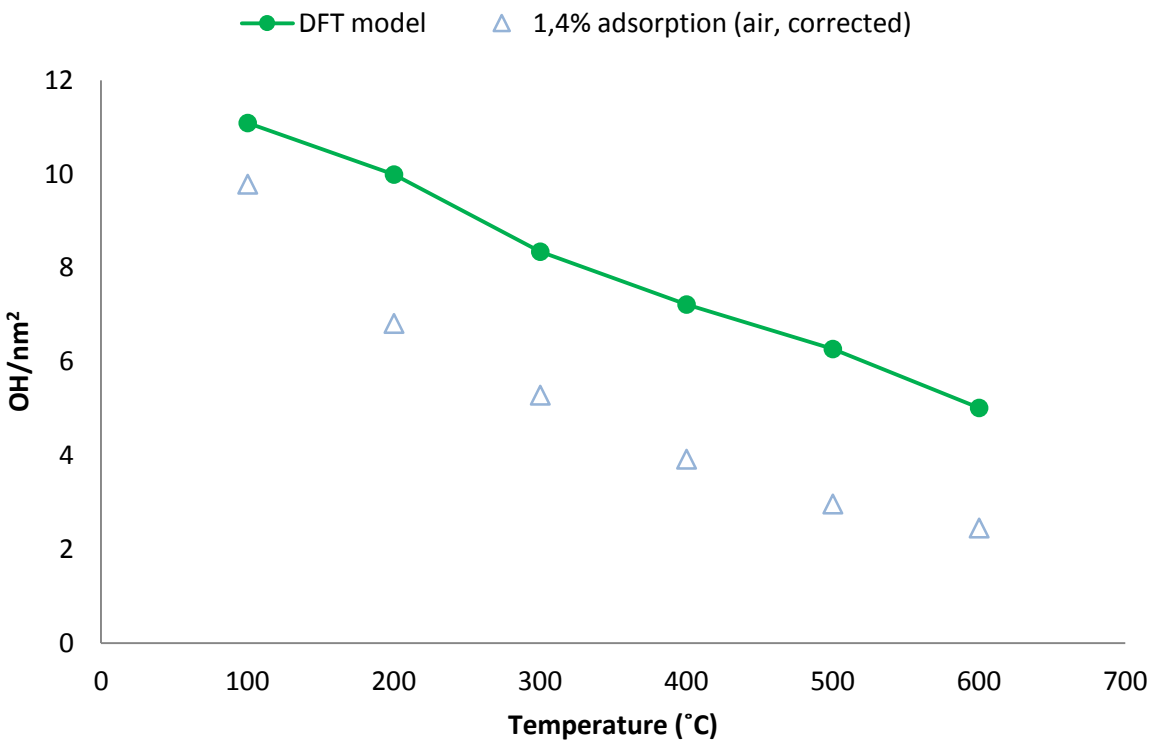

Figure 4.13 – Comparison between the experimental points for adsorption at 1400 Pa and the model based on DFT.

The Langmuir multisite model (4.7) is also taken into consideration to simulate the experimental values. However, to apply this model, it is necessary to know the number of adsorption sites and, for each of them, the maximum adsorbed quantity, the adsorption enthalpy and entropy. These parameters could be extracted from the simulated model based on DFT, but it would be a very onerous work, and as such this model is not considered.

$$n^a = n_m^a \frac{K_z P_A}{1 + \sum_z K_z P_z} \quad (4.7)$$

Where:

n^a – Adsorbed quantity (g/g);

n^a_m – Maximum adsorbed quantity (g/g);

z – Different adsorption sites considered;

K_z – Equilibrium constant;

$P_{A,Z}$ – Partial pressure for A and Z (Pa).

Another way to develop a representative and user friendly model exists. Knowing the coverage and the differential heat of adsorption, it is possible, using simple assumptions, to reach the differential energy distribution of the number of adsorption sites corresponding to adsorption energy ε by (4.8).

$$\int_\Omega f(\varepsilon) d(\varepsilon) = 1 \quad (4.8)$$

Where:

f(ε) – Differential energy distribution of the number of adsorption sites corresponding to a certain adsorption energy;

ε – Adsorption energy;

Ω – Domain of *ε*.

The overall coverage is given by (4.9).

$$\theta = \int_\Omega \theta(\varepsilon) f(\varepsilon) d(\varepsilon) \quad (4.9)$$

Where:

Θ – Overall coverage;

Θ(ε) – Coverage at the equilibrium on energetically homogeneous sites with adsorption energy *ε*.

As such, the associative adsorption on local sites with identical energy is of a monosite Langmuir type.

The key problem is to solve the integral (4.9) for different *f*(ε) for a specific coverage, especially to obtain the empirical isotherms dealing with chemisorption on a heterogeneous surface.

A way to reach the results is to use experimental isotherms, and extract the differential heat of adsorption or the molar heat of adsorption. With those values, it is possible to develop a predictive adsorption isotherms model.

In his thesis, Xia [61] developed several adsorption models, with one that represents well the experimental data (Figure 4.14): the normal-like distribution model, given by 4.10. The location parameter is approximately equal to the adsorption enthalpy, which is calculated using the Dima and Rees approach. The scale parameter is fitted using the model and experimental values. Finally, the standard variation of entropy is obtained by DFT calculations.

$$\theta = \frac{exp\left(\frac{T\Delta s^0+\epsilon_c}{\epsilon_v}\right)\left(\frac{p}{p^0}\right)^{RT/\epsilon_c}}{1+exp\left(\frac{T\Delta s^0+\epsilon_c}{\epsilon_v}\right)\left(\frac{p}{p^0}\right)^{RT/\epsilon_c}} \quad (4.10)$$

Where:

Θ – Overall coverage;

Δs^0 – Standard variation of entropy (kJ/mol);

ε_c – Location parameter;

ε_v – Scale parameter.

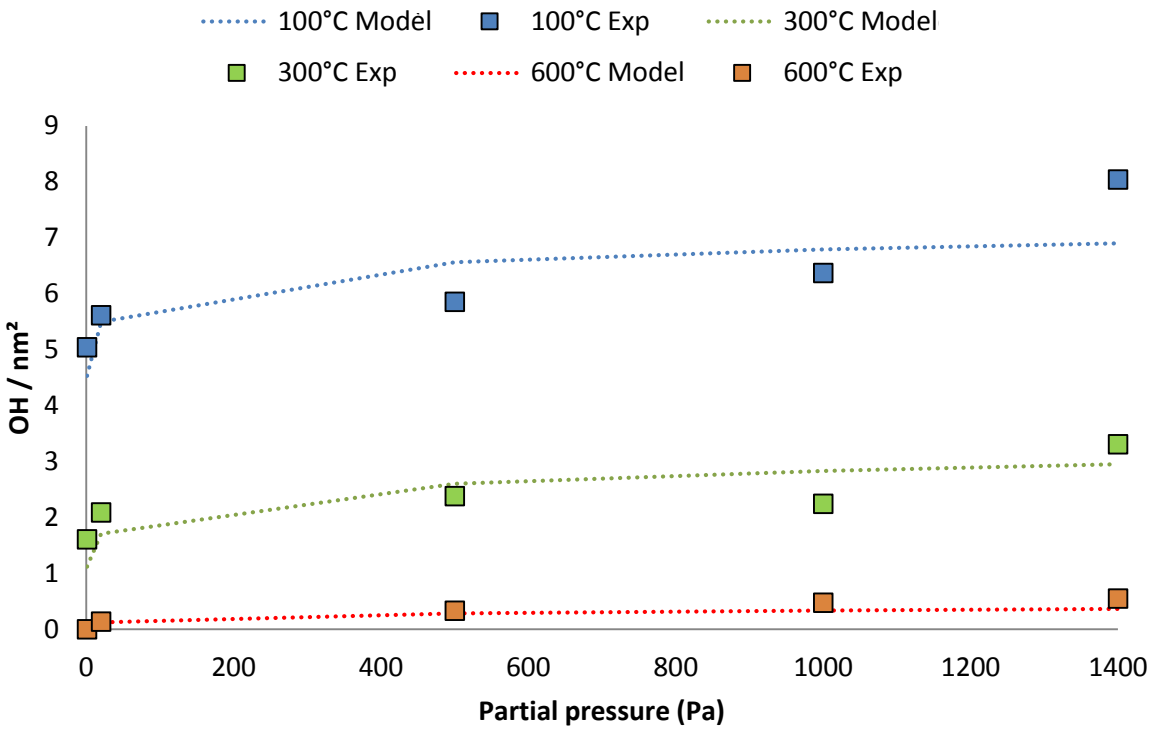

Figure 4.14 – Comparison between the experimental water adsorption isotherms for the reference sample and the normal-like distribution model.

Considering this good representation of the experimental data by the model, it is possible to conclude that the adsorption measurements can be simulated by this model. However, some points, especially at high partial pressures and low temperatures, deviate from the experimental ones. This could also be explained taking into account this kind of model is designed for chemisorption only; as such, there may be physisorption occurring at these conditions.

Thanks to this study, a procedure has been successfully set up to determine accurate water adsorption isotherms. Models for desorption curves and adsorption isotherms have also been developed so that it is now possible to extract important information, such as the adsorption enthalpy.

The same methodology will now be applied to the other samples prepared during this study.

4.1.2. Influence of the synthesis atmosphere

Sample #3 is synthesized by the thermal decomposition of Pural SB3 at 650°C for 6h under nitrogen with a water partial pressure of 230 Pa. The characteristics of the γ-alumina obtained are on Table 4.1. The corresponding XRD spectra (Figure 4.15) show that the alumina obtained is a γ-alumina, with coincident theoretical and experimental diffraction rays.

Table 4.3 – Most important characteristics of sample #3.

Analysis	Results
XRD	Figure 4.15
Specific surface area, S_{BET} (m^2/g)	233
NMR ^{27}Al (Al^{VI}/Al^{IV})	75/25

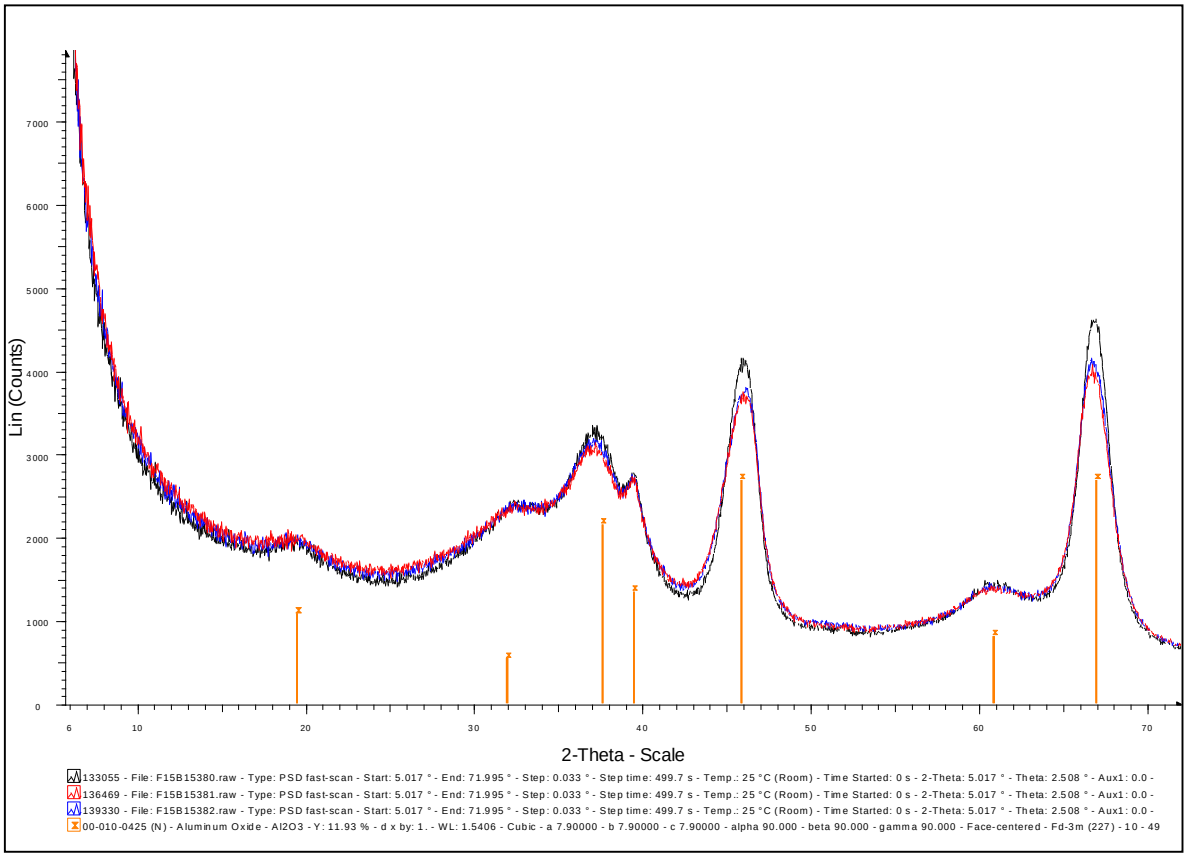

Figure 4.15 – XRD of sample #3 in red.

The only significant difference this sample has in comparison with the reference sample is its color, which is gray. To explain this, two hypotheses are formulated.

First, without oxygen in the synthesis gas, there could be some carbonaceous residue in the alumina, but by a CHONS analysis, it is verified that none of the samples contain an important carbon content (0,03% for this sample, and 0,06% for the reference one).

Secondly, it could be envisaged that some defects have been created because of the lack of oxygen in the system. This type of defects should be detectable by UV-vis analysis [62]. The UV-vis spectra of both samples synthesized under air and nitrogen are drawn in Figure 4.16. The characteristic band gap at 4,5 eV indicates the samples are γ-aluminas. However, it is clear the type of defects are dissimilar: the sample synthesized under nitrogen has more oxygen gaps, that can create defects at the surface, as well as center-F defects that are non-existent in the sample synthesized under air, creating a difference in charge that may be responsible for new types of defects.

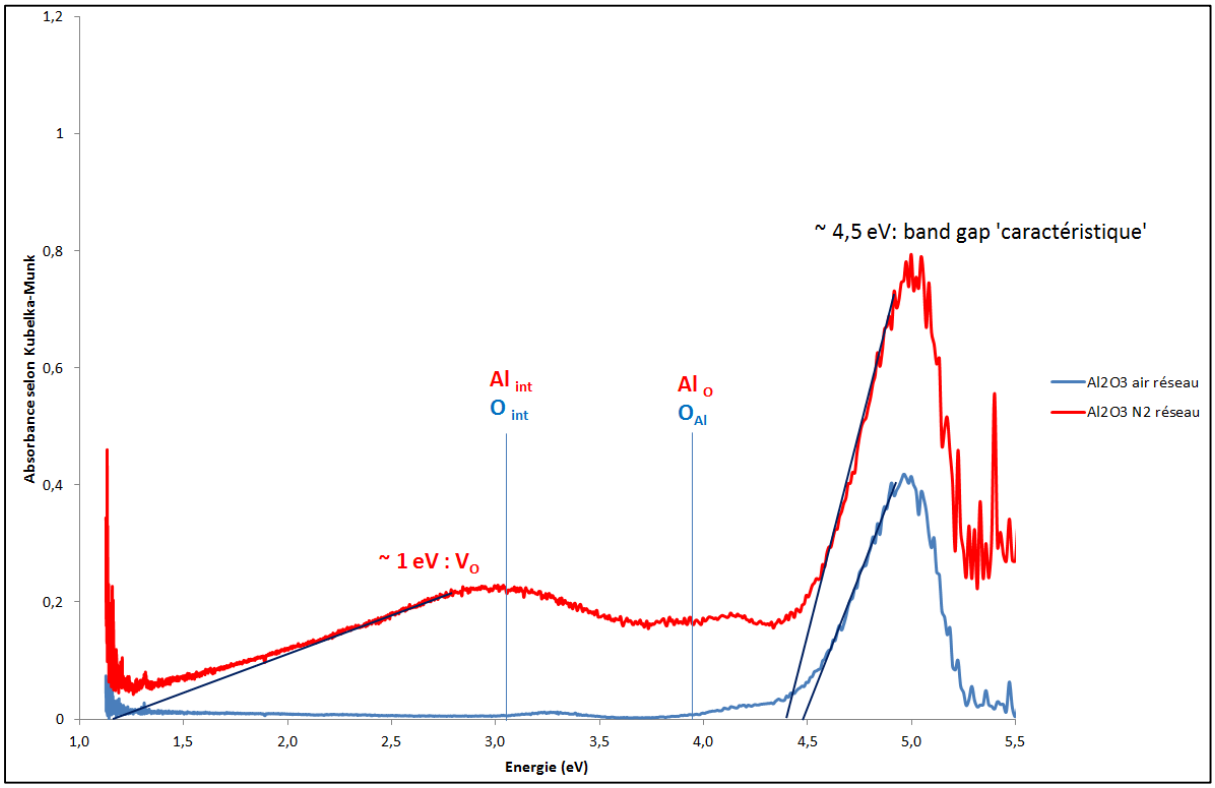

Figure 4.16 – UV-vis analysis of the reference sample and sample #3.

The presence of such oxygen vacancies seems a viable explanation for the higher adsorbed quantities of water deduced from desorption experiments at low temperatures for the sample synthesized under nitrogen compared to those for the sample prepared under air (Figure 4.17).

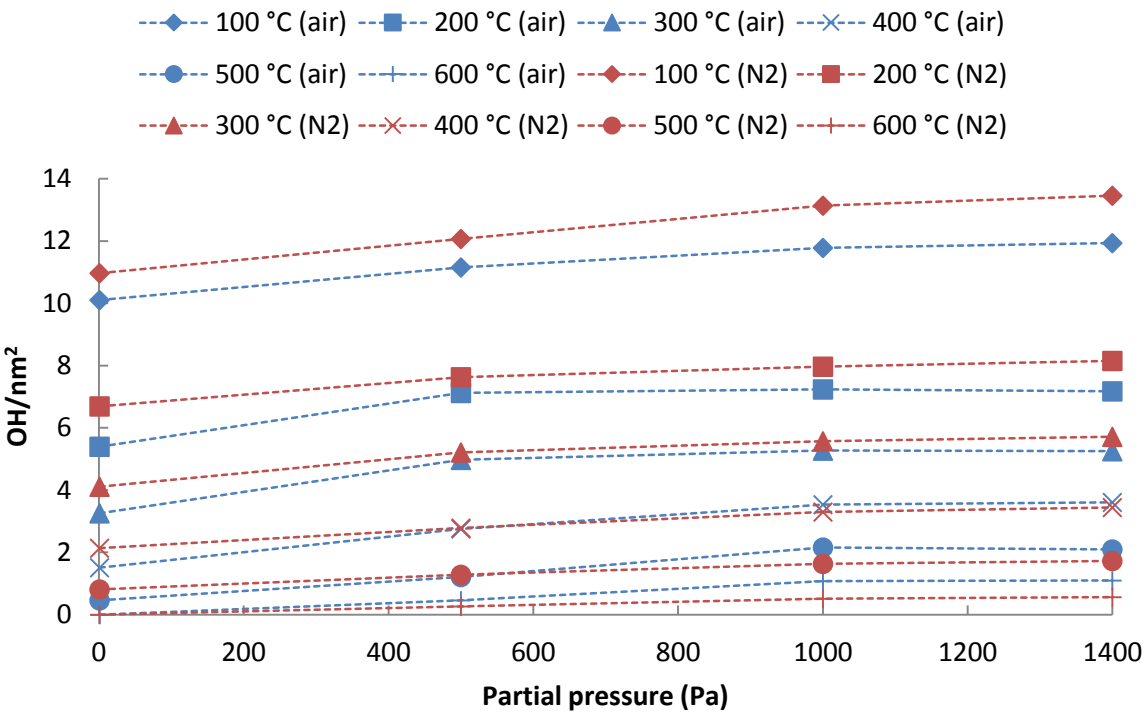

Figure 4.17 – Quantities of water adsorbed during desorption experiments for the reference sample and sample #3.

A study of the influence of a pretreatment step at 600°C on this sample is also done (Figure 4.18), where it can be seen that, unlike the sample synthesized under air, the pretreatment has a non-negligible effect on the desorption isobar, especially at low temperatures, with the pretreated sample having a lower surface coverage than the non-pretreated one.

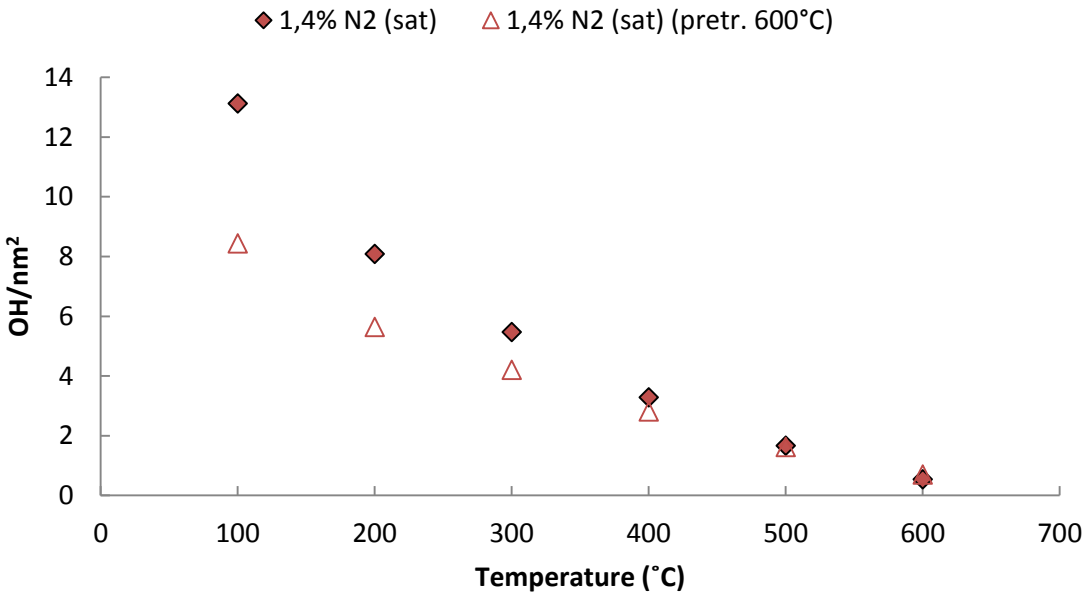

Figure 4.18 – Water desorption isobars at 1400 Pa with and without a pretreatment step for sample #3.

This implies that some oxygen gaps have been filled during the pretreatment, resulting in a sample that adsorbs less. Yet, as the pretreatment is done under nitrogen, the only explanation is that the atmosphere contains traces of oxygen that are enough to fill these vacancies. If this is true, the same kind of phenomena is expected to happen during the synthesis of alumina, with more or less vacancies being generated depending on the synthesis time. At the limit, the sample would have no oxygen vacancies if the synthesis time is long enough.

As such, an alumina is synthesized under nitrogen atmosphere during 12 h, twice the usual time, and the recovered powder is white, instead of gray. Consequently, the alumina synthesized under nitrogen is not a stable sample, since it continuously changes under atmosphere, and it would be too difficult to be sure of its surface state. Thus, it has been decided to give up nitrogen as a synthesis gas.

4.1.3. Influence of the boehmite morphology

Sample #5 is synthesized by the thermal decomposition of Disperal 40 at 650°C for 6h under air with a water partial pressure of 230 Pa. The characteristics of the γ-alumina obtained are on Table 4.4.

Table 4.4 – Most important characteristics of sample #5.

Analysis	Results
XRD	γ-alumina
Specific surface area, S_{BET} (m^2/g)	100

The adsorption and desorption measurements for this sample are obtained at a water partial pressure of 1400 Pa, and can be seen in Figure 4.19.

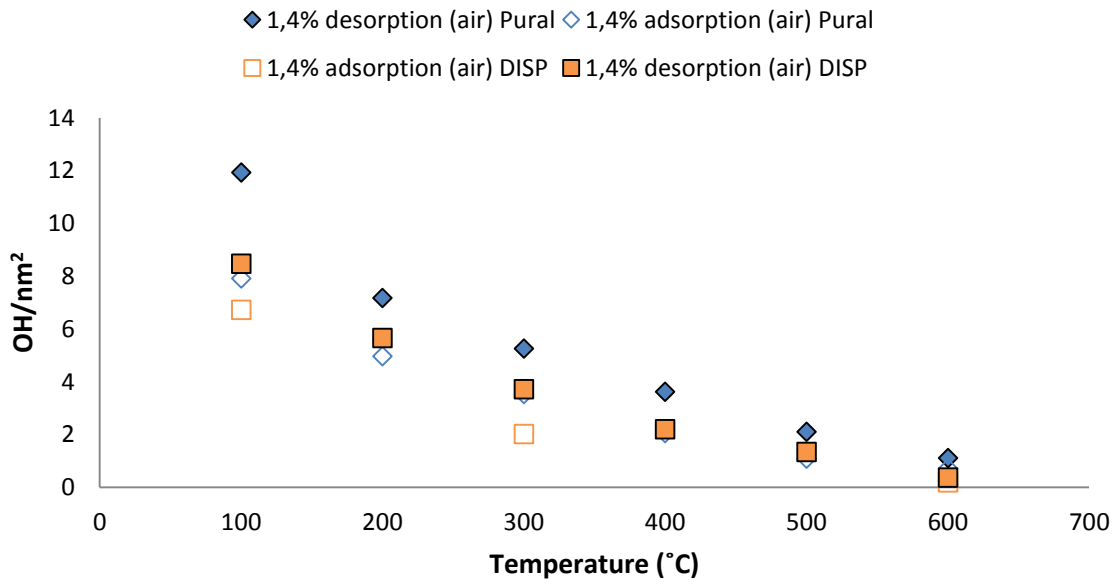

Figure 4.19 – Adsorption isobars for the reference sample and sample #5 at a water partial pressure of 1400 Pa.

It is apparent that this sample results in an alumina that adsorbs less than the reference sample, which was synthesized from Pural SB3, this difference being constant even at 600°C. This could be due to the fact that alumina from Disperal 40 has proportionally less edges than Pural SB3, which could be high energetic sites. By IR spectroscopy, it would be probably possible to get more precise information, but at the time of writing of this report, these analyses are in progress.

On the other hand, for the alumina from Disperal 40, the adsorbed quantities at 600°C obtained by desorption and adsorption experiments are almost identical and very close to zero. This seems to indicate that at this temperature and water partial pressure, the water is all desorbed from the surface of the sample, which is different from what happens to the reference one. This shows that the last desorption sites are less energetic than those of the reference. To confirm this, it is necessary to proceed to the estimation of the desorption activation energy for this sample, as it was done for the reference.

4.1.4. Comparison between the synthesized samples

Pural SB3 thermally decomposed under air with a water partial pressure of 240 Pa in order to obtain γ-alumina has been defined as a reference sample. Its hydration and dehydration have been extensively studied, and they lead to the conclusion that the last hydroxyls are very strongly linked to the surface and need a high activation energy to be desorbed. Thus, the only manner to reach adsorption equilibrium points is to proceed to adsorption experiments. This is reinforced by the good adjustment of adsorption isotherms by different models, one based on DFT calculations, and another statistical one. Moreover, although desorption experiments do not correspond to an equilibrium, their modelisation leads to the enthalpy of adsorption. Thanks to IR and ^{1}H NMR analyses, it has been shown that the last desorbed hydroxyls correspond to different types of hydroxyls. This suggests that to desorb one water molecule, the needed hydroxyl and hydrogen come from two different types of hydroxyls, with the hydrogen coming probably from a bridged hydroxyl.

To try to get other samples with different surface states, Pural SB3 has been thermally decomposed under nitrogen, but it leads to a sample with oxygen vacancies continuously varying even under this inert gas.

Another sample has been synthesized under air, but from boehmite Disperal 40, which results in an alumina with proportionally less edges compared to the alumina synthesized from the Pural SB3. Adsorption of water shows that this has a noticeable influence: this sample adsorbs less water, and has probably less energetic adsorption sites, since it is possible to remove all surface hydroxyls at 600°C.

The hydrocarbon adsorption capacities of these two aluminas with different surface states have now to be studied in order to try to establish a correlation between them.

4.2. Hydrocarbons adsorption

Due to lack of time, only the reference sample, alumina synthesized from Pural SB3 under air, has been tested in hydrocarbons adsorption. Ethane and ethylene are used in this work, since they are simple molecules that differ only in a double bond, as well as being relatively inexpensive.

The adsorption of ethylene is done at 30°C according to the program described in the Methods. The alumina is activated at temperatures from 100 to 600°C in 100°C increments under a nitrogen flow of 4 NL/l containing 1 Pa of water. Even if the desorption experiments do not reach a thermodynamic equilibrium, the stabilization state is sufficiently stable to use the desorption experiments to set up the hydration state of the sample before adsorbing hydrocarbons on them. Between each activation plateau, the alumina is submitted to a similar nitrogen flow, though this time containing an ethylene partial pressure of 0,25 bar. The results obtained can be seen in Figure 4.20. For comparison, there is a desorption point obtained for ethane during preliminary tests.

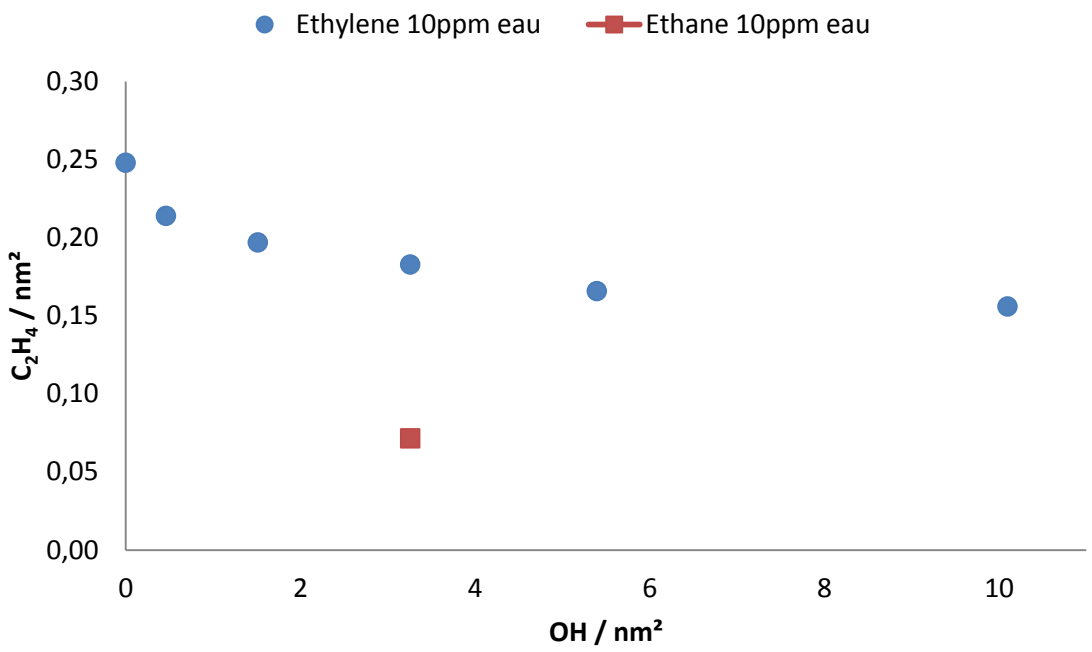

Figure 4.20 – Ethylene and ethane adsorbed on the reference sample in function of the surface coverage.

First, at the same surface coverage, ethylene adsorbs more than ethane. This goes with literature in the sense that adsorption is more favorable for unsatured hydrocarbons, in comparison with their linear equivalents [18].

Secondly, the quantity of adsorbed ethylene increases as the number of surface hydroxyls decreases; in other words, the more dehydroxylation, the more hydrocarbons adsorption is favored. Looking at ethylene adsorption at very low surface coverage, the shape of the curve also indicates that desorption of the very last hydroxyls may create more specific sites for ethylene adsorption. Nonetheless, the nature of the sites needs now to be identified.

5. Conclusions and future work

In this work, different γ-alumina samples were synthesized by varying their synthesis conditions. A reference sample was synthesized from boehmite Pural SB3 under air with a water partial pressure of 240 Pa. To compare the influence of the synthesis gas, another sample was synthesized in a similar fashion to the reference, but using nitrogen instead of air. Unfortunately, it lead to an unstable sample. To compare the influence of the boehmite morphology, another sample was synthesized similarly, but using boehmite Disperal 40, which has a lower ratio of edges and plans compared to Pural SB3. As such, it was possible to obtain different γ-alumina surfaces.

For the reference sample, a procedure was successfully set up to determine accurate water adsorption isotherms. Indeed, its hydration and dehydration were extensively studied, leading to the conclusion that the last hydroxyls are very strongly linked to the surface and need a high activation energy to be desorbed. Thus, the only way to reach adsorption equilibrium points was to proceed to adsorption experiments, which was reinforced by the good adjustment of adsorption isotherms by different models, one based on DFT calculations, and another statistical one. Moreover, although desorption experiments do not correspond to an equilibrium, their modelisation lead to the enthalpy of adsorption. Thanks to IR and ^{1}H NMR analyses, it was shown that the last desorbed hydroxyls correspond to different types of hydroxyls. This suggests that to desorb one water molecule, the needed hydroxyl and hydrogen come from two different types of hydroxyls, with the hydrogen coming probably from a bridged hydroxyl.

For the use of a boehmite with a lower ratio between the edges and plans, it was possible to see that this resulted in a sample that has a lower number of adsorption sites, since the edges correspond to high energetic adsorption sites. The sites in this sample were also less energetic than the reference, since it was possible to remove all the water at the surface at a water partial pressure of 1400 Pa and 600°C.

As such, it was possible to synthesize two different γ-alumina surfaces with different water adsorption properties, and to correlate them with the synthesis conditions.

The study on hydrocarbons adsorption on γ-alumina was also started on the reference sample. It was found that ethylene adsorbs more than ethane at the same conditions. Also, ethylene adsorption depended on the surface coverage of γ-alumina, increasing with its decrease. At very low surface coverage, the shape of the isotherm seemed to indicate that there is the formation of more specific sites, since ethylene adsorption increased more in that area.

Regarding the very encouraging results obtained by this study, this work has to be continued. First, the sample synthesized from Disperal 40 has to be analyzed by IR and ^{1}H NMR spectroscopies to try to identify the types of surface hydroxyls missing compared to the sample synthesized from Pural SB3. Then, its hydrocarbons adsorption adsorption capacities have to be determined. By comparing all these results with those of the sample synthesized from Pural SB3, some links could probably be established between surface state and adsorption of hydrocarbons. Afterwards, it would also be interesting to consider obtaining another γ-alumina surface, maybe by using another boehmite.

References

1. Lower S: **Catalysts. Catalysts reduce activation energy,** no date. *Retrieved from:* http://chemwiki.ucdavis.edu/Physical_Chemistry/Kinetics/Complex_Reactions/Catalysis/Catalysts [accessed on 08/2015].
2. Wefers K, Misra C: *Oxides and Hydroxydes of Aluminum*; Alcoa Laboratories; 1987.
3. Koerin R: **Influence du mode de synthèse de la boehmite sur l'état de surface de l'alumine-γ mise en forme; application au reformage catalytique,** IFPEN; 2015.
4. Alphonse P, Courty M: **Structure and thermal behavior of nanocrystalline boehmite**. *Thermochim. Acta* 2005, **425**:75-89.
5. Ostwald W: *Lehrbuch der Allgemeinen Chemie*; Engelmann; 1896.
6. Trueba M, Trasatti P: **γ-Alumina as a support for catalysts: a review of fundamental aspects**. *Eur. J. Inorg. Chem.* 2005, **2005**:3393-3403.
7. Tsyganenko A, Mardilovich P: **Structure of alumina surfaces**. *J. Chem. Soc.* 1996:4843-4852.
8. Pecharromán C, Sobrados I, Iglesias JE, González-Carreño T, Sanz J: **Thermal evolution of transitional aluminas followed by NMR and IR spectroscopies**. *J. Phys. Chem. B* 1999, **103**:6160-6170.
9. Sohlberg K, Pennycook J, Pantelides T: **Explanation of the observed dearth of three-coordinated Al on γ-alumina surfaces**. *J. Am. Chem. Soc.* 1999, **121**:10999-11001.
10. Paglia G, Buckley E, Udovic T, Rohl L, Jones F, Maitland F, Connolly J: **Boehmite-derived γ-alumina system, 2. Consideration of hydrogen and surface effects**. *Chem. Mater.* 2004, **16**:1914-1923.
11. González-Peña V, Díaz I, Márquez-Alvarez C: **Thermally stable mesoporous alumina synthesized with non-ionic surfactants in the presence of amines**. *Micropor. Mesopor. Mat.* 2001, **44-45**:203-210.
12. Bhattacharya A, Pyke D, Walker G, Werrett C: **The surface reactivity of different aluminas as revealed by their XPS C1s spectra**. *Appl. Surf. Sci.* 1997, **108 (4)**:465-470.
13. Lippens B, Boer J: **Study of phase transformations during calcination of aluminum hydroxides by selected area electron diffraction**. *Acta Cryst.* 1964, **17**:1312-1321.
14. Marcilly C: **L'alumine support de catalyseurs acides ou bifonctionnels: synthèse, structures, texture et modèles de surface,** IFPEN; 1993.
15. Wang A, Bokhimi X, Morales A, Novaro O, López T, Gómez R: **Aluminum local environment and defects in the crystalline structure of sol−gel alumina catalyst**. *J. Phys. Chem. B* 1999, **103**:299-303.
16. Wang Y, Bronsveld P, DeHosson J, Djuricic B, McGarry D, Pickering S: **Ordering of octahedral vacancies in transition aluminas**. *J. Am. Ceram. Soc.* 1998, **81**:1655-1660.
17. Wilson S: **Dehydration of boehmite, γ-AlOOH, to γ-Al2O3**. *J. Solid State Chem.* 1979, **30**:247-255.
18. Wilson S, McConnel J: **A kinetic study of the system α-AlOOH-Al2O3**. *J. Solid State Chem.* 1980, **34**:315-322.
19. Ionescu A, Allouche A, Aycard J, Rajzmann M, Hutschka F: **Study of γ-alumina surface reactivity: adsorption of water and hydrogen sulfide on octahedral aluminum sites**. *J. Phys. Chem. B* 2002, **106**:9359-9366.
20. Busca G: **Spectroscopic characterization of the acid properties of metal oxide catalysts**. *Catal. Today* 1998, **41**:191-206.
21. Coster D, Fripiat J, Muscas M, Auroux A: **Effect of bulk properties on the rehydration behavior of aluminas**. *Langmuir* 1995, **11**:2615-2620.
22. Coster D, Fripiat J: **Memory effects in gel-solid transformations: coordinately unsaturated aluminum sites in nanosized aluminas**. *Chem. Mater.* 1993, **5**:1204-1210.
23. Morterra C, Magnacca G: **A case study: surface chemistry and surface structure of catalytic aluminas, as studied by vibrational spectroscopy of adsorbed species**. *Catal. Today* 1996, **27**:497-532.

24. Knözinger H, Ratnasamy P: **Catalytic aluminas: surface models and characterization of surface sites**. *Catal. Rev.* 1978, **17**:31-70.
25. Digne M, Sautet P, Raybaud P, Euzen P, Toulhoat H: **Hydroxyl groups on γ-alumina surfaces: a DFT study**. *J. Catal.* 2002, **211**:1-5.
26. Digne M: **Use of DFT to achieve a rational understanding of acid-basic properties of γ-alumina surfaces**. *J. Catal.* 2004, **226**:54-68.
27. Henriques C: **Análise do ciclo catalítico heterogéneo;** IST, no date.
28. Sing K: **Reporting physisorption data for gas-solid systems**. *Pure Appl. Chem.* 1982, **54**:2201-2218.
29. Christmann K: *Modern methods in heterogeneous catalysis research;* Freie Universität*,* 2010.
30. Naeem R: **Lennard-Jones potential,** no date. *Retrieved from:* http://chemwiki.ucdavis.edu/Physical_Chemistry/Physical_Properties_of_Matter/Intermolecular_Forces/Lennard-Jones_Potential [accessed on 08/2015].
31. Adamson A, Gast A, Adamson W, Gast P: *Physical Chemistry of Surfaces;* Wiley-Interscience; Wiley; 1997.
32. Langmuir I: **The constitution and fundamental properties of solids and liquids**. *J. Am. Chem. Soc.* 1916, **38**.
33. Sun L, Meunier F, Baron G: **Adsorption - Procédés et applications;** TD Ed., 2005.
34. Brunauer S, Emmett P, Teller E: **Adsorption of gases in multimolecular layers**. *J. Am. Chem. Soc.* 1938, **60**:309-319.
35. Coster D, Fripiat J, Muscas M, Auroux A: **Effect of bulk properties on the rehydration behavior of aluminas**. *Langmuir* 1995, **11**:2615-2620.
36. Desai R, Hussain M, Ruthven D: **Adsorption of water vapour on activated alumina. I -- Equilibrium behaviour**. *Can. J. Chem. Eng.* 1992, **70**:699-706.
37. Kim J, Lee C, Kim W, Lee J, Suh J: **Adsorption equilibria of water vapor on alumina, zeolite 13X, and a zeolite X/activated carbon composite**. *J. Chem. Eng. Data* 2003, **48**:137-141.
38. Ruiz J, Pinto J, Masiá A, Paniego A: **Thermodynamics of the adsorption of hydrocarbons on alumina**. *J. Chem. Thermodyn.* 1986, **18**:903-914.
39. Grebenkemper J: **Powder X-ray Diffraction. Instrumentation**, no date. *Retrieved from:* http://chemwiki.ucdavis.edu/Analytical_Chemistry/Instrumental_Analysis/Diffraction/Powder_X-ray_Diffraction [accessed on 08/2015].
40. Birkner N, Wang Q: **How an FTIR spectrometer operates**, no date. *Retrieved from:* http://chemwiki.ucdavis.edu/Physical_Chemistry/Spectroscopy/Vibrational_Spectroscopy/Infrared_Spectroscopy/How_an_FTIR_Spectrometer_Operates [accessed on 08/2015].
41. Keeler J: **Understanding NMR spectroscopy**; University of Cambridge, 2002.
42. Brown K: **Pulse Sequences**, no date. *Retrieved from:* http://chemwiki.ucdavis.edu/Physical_Chemistry/Spectroscopy/Magnetic_Resonance_Spectroscopies/Nuclear_Magnetic_Resonance/NMR%3A_Experimental/Pulse_Sequences [accessed on 08/2015].
43. Reusch W: **UV-Visible Spectroscopy**, no date. *Retrieved from:* https://www2.chemistry.msu.edu/faculty/reusch/VirtTxtJml/Spectrpy/UV-Vis/spectrum.htm [accessed on 08/2015].
44. Thomas M, Bounie C: **Manuel operatoire Thermobalance Setaram TAG-B12;** IFPEN, 2010.
45. Johnson M: **Surface area stability of aluminas**. *J. Catal.* 1990, **123**:245-259.
46. Vargaftik N, Volkov B, Voljak L: **International tables of the surface tension of water**. *J. Phys. Chem. Ref. Data* 1983, **12**.
47. Dima E, Rees L: **Temperature programmed desorption of sorbates from zeolites. Part 2: New analytical method testes on dehydration of dealuminated Y zeolites**. *Zeolites* 1987, **3**:219-227.
48. Hendriksen B, Pearce D, Rudham R: **Heats of adsorption of water on α- and γ-alumina**. *J. Catal.* 1972, **24**:82-87.

49. Marsh K: *Recommended Reference Materials for the Realization of Physicochemical Properties.* Oxford: Blackwell Publishing; 1987.
50. Taoufik M, Szeto K, Merle N, Rosal I, Maron L, Trébosc J, Tricot G, Gauvin R, Delevoye L: **Heteronuclear NMR spectroscopy as surface-selective technique: a unique look at the hydroxyl groups of γ-alumina**. *Chem. Eur. J.* 2014, **20**.
51. Kohn W, Sham L: **Self-Consistent Equations Including Exchange and Correlation Effects.** *Phys. Rev. A* 1965, **140**:1133-1138.
52. Hohenberg P, Kohn W: **Inhomogeneous Electron Gas.** *Phys. Rev. B* 1964:864-871.
53. Sabbe M, Reyniers M, Reuter K: **First-principles kinetic modeling in heterogeneous catalysis: an industrial perspective on best-practice, gaps and needs.** *Catal. Sci. Technol.* 2012, **2**:2010-2024.
54. Kresse G, Furthmüller: **Efficiency of ab-initio total energy calculations for metals and semiconductor using a plane-wave basis set.** *J. Comp. Mat. Sci.* 1996, **6**:15-50.
55. Kresse G, Hafner: **Ab-initio molecular-dynamics simulation of the liquid-metal--amorphous-semiconductor transition in germanium.** *J. Phys. Rev. B* 1994, **49**:14251-14269.
56. Digne M, Sautet P, Raybaud P, Euzen P, Toulhoat H: **Hydroxyl groups on γ-alumina surfaces: a DFT study**. *J. Catal.* 2002, **211**:1-5.
57. Digne M: **Use of DFT to achieve a rational understanding of acid-basic properties of γ-alumina surfaces**. *J. Catal.* 2004, **226**:54-68.
58. Wischert R, Laurent P, Copéret C, Delbecq F, Sautet P: **γ-alumina: The Essential and Unexpected Role of Water for the Structure, Stability, and Reactivity of "Defect" Sites.** *J. Am. Chem. Soc.* 2012, **134**:14430-14449.
59. Lamier K, Chizallet C, Cadran N, Maury S, Abboud J, Lamic-Humblot A, Marceau E, Lauron-Pernot H: **Mechanistic Investigation of Isopropanol Conversion on Alumina Catalysts: Location of Active Sites for Alkene/Ether Production.** *ACS Catalysis* 2015, **5**:4423-4437.
60. Xia X: **Experimental and theoretical aspects of adsorption microcalorimetry applied to characterize heterogeneous catalysts**; 2006.
61. Keeler J: *Understanding NMR spectroscopy*; Wiley, 2010.
62. Ruiz J, Pinto J, Masiá A, Paniego A: **Thermodynamics of the adsorption of hydrocarbons on alumina**. *J. Chem. Thermodyn.* 1986, **18**:903-914.